Title

Model Predictive Control of a Nonlinear Large-Scale Process Network Used in the Production of Vinyl Acetate

Author

Tu, TungSheng

Publication Date

2013

Peer reviewed|Thesis/dissertation

UNIVERSITY OF CALIFORNIA

Los Angeles

Model Predictive Control of a Nonlinear Large-Scale Process Network Used in the Production of Vinyl Acetate

A thesis submitted in partial satisfaction of the
requirements for the degree Master of Science
in Chemical Engineering

by

TungSheng Tu

2013

ABSTRACT OF THE THESIS

Model Predictive Control of a Nonlinear Large-Scale Process Network
Used in the Production of Vinyl Acetate

by

TungSheng Tu

Master of Science in Chemical Engineering
University of California, Los Angeles, 2013
Professor Panagiotis D. Christofides, Chair

In this work, we focus on the development and application of two Lyapunov-based model predictive control (LMPC) schemes to a large-scale nonlinear chemical process network used in the production of vinyl acetate. The nonlinear dynamic model of the process consists of 179 state variables and 13 control (manipulated) inputs and features a cooled plug-flow reactor, an eight-stage gas-liquid absorber, and both gas and liquid recycle streams. The two control schemes considered are an LMPC scheme which is formulated with a convectional quadratic cost function and a Lyapunov-based economic model predictive control (LEMPC) scheme which is formulated with an economic (non-quadratic) cost measure. The economic cost measure for the entire process network accounts for the reaction selectivity and the product separation quality. In the LMPC and LEMPC control schemes, five inputs, directly affecting the economic cost, are regulated with LMPC/LEMPC and the remaining eight inputs are computed by proportional-integral controllers. Simulations are carried out to study the economic performance of the closed-loop system under LMPC and under LEMPC formulated with the proposed economic measure. A thorough comparison of the two control schemes is provided.

The thesis of TungSheng Tu is approved.

Gerassimos Orkoulas

James F. Davis

Panagiotis D. Christofides, Committee Chair

University of California, Los Angeles

2013

Contents

List of Figures

List of Tables

Nomenclature

Roman Symbols

a_i Vapor heat capacity/enthalpy coefficient for species i — $kcal/kg°C$

$\bar{a}_i$ Liquid heat capacity/enthalpy coefficient for species i — $kcal/kg°C$

$\tilde{a}_{ij}$ Wilson parameters of species pair i-j — $kcal/kmol$

$\tilde{A}_i$ Antoine coefficent of species i

b_i Vapor heat capacity/enthalpy coefficient for species i — $kcal/kg°C^2$

$\bar{b}_i$ Liquid heat capacity/enthalpy coefficient for species i — $kcal/kg°C^2$

$\tilde{B}_i$ Antoine coefficient of species i

c_i Vapor concentration of species i — $kmol/m^3$

$\check{c}_i$ Liquid heat capacity of species i — $kcal/kmol°C$

$\hat{c}_i$ Vapor heat capacity of species i — $kcal/kmol°C$

C Total vapor concentration — $kmol/m^3$

$\check{C}$ Liquid heat capacity — $kcal/kmol°C$

$\hat{C}$ Vapor heat capacity — $kcal/kmol°C$

$\tilde{C}_i$ Antoine coefficient of species i

f Vapor molar flow rate	$kmol/min$
$\bar{f}$ Liquid molar flow rate	$kmol/min$
h_i Vapor enthalpy of species i	$kcal/kmol$
$h_{L,i}$ Latent heat of species i	$kcal/kmol$
$h_{rxn,i}$ Heat of the ith reaction ($i = 1, 2$)	$kcal/kmol$
$\bar{h}_i$ Liquid enthalpy of species i	$kcal/kmol$
H Vapor phase enthalpy	$kcal/kmol$
$\bar{H}$ Liquid phase enthalpy	$kcal/kmol$
k Mass transfer coefficient	$kmol/min$
K Equilibrium constant	
M Total moles in vapor phase	$kmol$
$\bar{M}$ Total moles in liquid phase	$kmol$
MW_i Molecular weight of species i	$kg/kmol$
$\bar{n}$ Mass transfer rate to the liquid phase	$kmol/min$
N_i Mass transfer rate of species i	$kmol/min$
p_i Partial pressure of species i	$psia$
p_i^{sat} Saturated pressure of species i	$psia$
P Pressure	$psia$
q Heat rate supplied or removed per unit volume	$kcal/m^3min$
Q Heat rate supplied or removed	$kcal/min$

Q_{tr} Convective heat transfer rate due to transferring materials $kcal/min$

SpG_i Specific gravity of species i

T Vapor temperature $^\circ C$

$T_{coolant}$ Coolant temperature $^\circ C$

$\bar{T}$ Liquid temperature $^\circ C$

UA Overall heat transfer coefficient $kcal/min^\circ C$

$\bar{U}$ Overall heat transfer coefficient per unit volume $kcal/m^3 min^\circ C$

$\bar{v}$ Liquid volume m^3

$\check{v}$ Superficial velocity m/min

$\tilde{v}_i$ Molar volume of species i $L/kmol$

W_s Actual work supplied to the compressor $kcal/kmol$

$\check{x}_i$ Liquid mole fraction of species i $kmol/kmol$

$\check{y}_i$ Vapor mole fraction of species i $kmol/kmol$

z Axial coordinate along the length m

Greek Symbols

$\tilde{\alpha}$ Fraction of stream in vapor phase

ϵ Catalyst porosity

γ_i Activity coefficient of species i

Λ_{cat} Catalyst heat capacity $kcal/kg^\circ C$

ρ_{cat} Catalyst density kg/m^3

$\zeta_{j,i}$ Stoichiometric coefficients for species i and reaction j, $j = 1, 2$

Subscripts

0 Inlet stream of the absorber or the plug-flow reactor

i Component ($i = C_2H_4$, O_2, HAc, VAc, CO_2, H_2O, C_2H_6)

int Vapor-liquid interface

j Stream number ($j = S1$, $S2$, ..., $S34$)

l Section number of the plug-flow reactor $l = 1, 2, \ldots, 10$ or theoretical stage number of the absorber $l = 1, 2, \ldots, 8$

max Maximum

net Net amount

b Absorber base

Superscripts

j Vessel number (j)

Acknowledgements

I would like to thank my advisor, Professor Panagiotis Christofides, for his tremendous guidance and support on the project. Also, many thanks to Prof. Gerassimos Orkoulas and Prof. James Davis, for being on my Master's thesis committee. Specifically, I am very grateful to gain tremendous help from Mathew Ellis on the project. At the end, it is the greatest thing ever to have a such supportive family.

Chapter 1

Introduction

1.1 Background

Vinyl acetate is mostly used in manufacturing polyvinyl acetate and other vinyl acetate co-polymers. Polyvinyl acetate is the fundamental ingredient for polyvinyl alcohol and polyvinyl acetate resins. Three raw materials, ethylene (C_2H_4), oxygen (O_2), acetic acid (HAc), react to form the desired product vinyl acetate (VAc) as well as two byproducts: carbon dioxide (CO_2) and water (H_2O). An inert component, ethane (C_2H_6), enters the process with the ethylene feed stream. The exothermic and irreversible gas phase chemical reactions are:

$$\begin{array}{ccc} C_2H_4 + HAc + \frac{1}{2}O_2 & \xrightarrow{r_1} & VAc + H_2O \\ C_2H_4 + 3O_2 & \xrightarrow{r_2} & 2CO_2 + 2H_2O \end{array} \tag{1.1}$$

where the heat of the ith reaction ($h_{rxn,i}$, $i = 1, 2$) are $h_{rxn,1} = -42100\ kcal/kmol$ and $h_{rxn,2} = -316000\ kcal/kmol$, respectively.

The fundamental challenge of controlling a vinyl acetate process network is operating a highly nonlinear coupled process at an economically optimal steady-state. Luyben and Tyreus [20, 22] presented a detailed process network design for manufacture of vinyl acetate monomer and demonstrated that plantwide control of the process can be accomplished by using a conventional proportional-integral (PI) control scheme. Chen et al. [5] developed

a nonlinear dynamic model of a vinyl acetate process in MATLAB based on Luyben and Tyreus's work, proposed a different control structure using combination of proportional (P) control and PI control loops, and studied the dynamics of the closed-loop system under several set-point changes and disturbances. Oslen et al. [30] proposed modified control structures, specifically focused on improving the liquid inventory system control and the controllability of the azeotropic distillation column using a feed-forward model predictive controller and a static ratio controller. Subsequently, Luyben [21] modified and optimized a vinyl acetate process flowsheet using the original unit operations presented in the previous work [20] from a steady-state economic point of view using Aspen Dynamics$^{\text{TM}}$.

Optimizing chemical processes from an economic perspective is an issue of primary importance in industry. The economic optimization of chemical processes is usually realized via a two-layer real-time optimization (RTO) system [24]. In an RTO system, the upper layer utilizes a steady-state process model to compute economically optimal process operation set-points while feedback control systems are used to force the system to track the set-points in the lower layer. MPC is usually adopted in the lower layer due to its ability of taking advantage of a dynamic model of the process to predict its future evolution along a given prediction horizon. MPC solves an on-line optimization problem to compute optimal control inputs by optimizing a quadratic cost function involving penalties on the deviation of the state and controlled variables from a desired steady-state while taking state and input constraints into account [10, 25]. Lyapunov-based MPC (LMPC) provides an explicit characterization of the stability region through utilization of a pre-existing Lyapunov-based controller as an auxiliary controller [27, 28, 26]. Recently, a significant number of efforts have been devoted to integrating MPC and economic optimization of chemical processes in order to manipulate process capacities in response to fast-changing global market demand [2, 16, 31]. Furthermore, the development of MPC with a general economic cost function has been studied in refs [7, 9, 12, 14, 1]. For example, two economically oriented nonlinear MPC formulations using Lyapunov techniques to guarantee nominal stability of the

closed-loop system for cyclic processes were studied in ref [14]. In refs [7, 1], MPC schemes using an economic-based cost function with established stability properties via a proper Lyapunov function were proposed, in which an incorporated terminal constraint ensures that the closed-loop system is driven to a steady-state at the end of the prediction horizon. Even though a rigorous stability analysis is discussed in ref [7], it is difficult, in general, to characterize, a priori, the set of initial conditions starting from where feasibility and closed-loop stability (both boundedness and convergence to a potentially economically optimal steady-state) of the proposed MPC are guaranteed. In contrast, a design of economic model predictive control (EMPC) using Lyapunov-based techniques (LEMPC) is able to optimize closed-loop performance with guaranteed stability with respect to general economic considerations for nonlinear systems [12].

Economic model predictive control has been applied to several applications [29, 15, 23]. In ref [23], energy costs in a commercial building were effectively reduced via an economic model predictive control technique with a shrinking prediction horizon; likewise, maximizing revenue from a dispatch-capable integrated gasification combined cycle (IGCC) was studied by using infinite-horizon economic model predictive control in ref [29].

Even though plantwide control designs using conventional control techniques on a vinyl acetate process have been extensively studied, application of model predictive control to a vinyl acetate process network has not been addressed in the literature. Motivated by this, we apply two model predictive control (MPC) schemes to a large-scale vinyl acetate process network: LMPC formulated with a conventional quadratic cost and LEMPC formulated with an economic measure which accounts for the reaction selectivity in the plug-flow reactor and vinyl acetate separation quality in the separator and the absorber. Closed-loop simulations of the vinyl acetate process network with both MPC schemes are carried out to study the closed-loop economic performance as well as compare the two MPC schemes. In the following sections, we introduce the process model which consists of 179 nonlinear ordinary differential equations and 13 manipulated inputs featuring a cooled plug-flow reactor,

an eight-stage gas-liquid absorber, and both gas and liquid streams. Next, we formulate the two control schemes for the vinyl acetate process network where the MPC schemes are used to regulate 5 manipulated inputs and a set of PI controllers are used regulate the remaining manipulated inputs to maintain closed-loop stability. Lastly, we present closed-loop simulation results and provide a thorough discussion on the comparison between the two control schemes.

1.2 Thesis structure

The thesis is organized as follows: chapter 2 describes the vinyl acetate process network and introduce the nonlinear dynamics of operation units in the process network. In chapter 3, we initially present a novel economic measure which is used in the formulation of the LEMPC and used to assess the economic performance of the closed-loop system under LMPC. Next, we provide a detailed description of the controller synthesis. Subsequently, we introduce the formulations of the Lyapunov-based model predictive control and Lyapunov-based economic model predictive control schemes formulated for the vinyl acetate process network. Chapter 4 provides thorough comparison of the two control schemes: LMPC and LEMPC. Chapter 5 concludes the project.

Chapter 2

Nonlinear vinyl acetate process network

2.1 Process description

The vinyl acetate process network flow diagram is shown in Figure 2.1. The process network is composed of several operation units including a vaporizer (VAP), a plug-flow reactor (RCT), a heat exchanger (HX), a separator (SEP), a compressor (COM), an absorber (ABS), and an acetic acid hold-up tank (TK). In addition to those main operation units, there are a total two heaters ($H1$ and $H2$) and three coolers ($C3$, $C4$, and $C5$) prior to the main operation units as shown in Figure 2.1. Using first principles, a nonlinear process model is obtained for each of these operation units. The carbon dioxide removal unit and the azeotropic distillation in Figure 2.1 are assumed to be component splitters with fixed CO_2 removal efficiency and VAc product recovery ratios, respectively.

An ethylene gas feed stream (S1) enters the process and is mixed with a preheated gas recycle stream (S34). The resulting mixed gas stream (S2) enters the vaporizer along with the acetic acid liquid recycle stream (S3) from the acetic acid hold-up tank. The exit gas stream (S4) from the vaporizer is further heated to a desired reactor inlet temperature.

To keep the oxygen composition in the gas recycle loop below the explosive region while providing sufficient oxygen for the reactions, oxygen is fed prior to the reactor (S5). The catalytic packed bed plug-flow reactor gas effluent (S8) enters the heat exchanger as the hot-side stream. The hot-side effluent from the heat exchanger (S9) is partially condensed through a pressure let-down valve and a cooler. In the separator, the exit liquid stream (S13) consists of mostly heavy components such as VAc, H_2O, and HAc; the exit vapor stream (S12) passes through a compressor and a heater before it enters the absorber where the remaining heavy components are further recovered and light components such as O_2, CO_2, C_2H_4, and C_2H_6 are recycled. A large portion of liquid from the base of the absorber is recirculated through a cooler and fed to the second stage of the absorber. The liquid effluents from the separator (S13) and the absorber (S17) are mixed and fed to an azeotropic distillation column in which the overhead stream (S26) contains the final product, vinyl acetate, of the process network. The liquid product from the bottom of the distillation column (S24) enters an acetic acid hold-up tank where the fresh acetic acid is also fed. A portion of liquid in the tank (S23) is pumped to the top stage of the absorber to provide final gas scrubbing. The overhead gas leaving the absorber (S16) is split and part of the stream (S27) with constant molar flow rate of $6.556\,kmol/min$ enters the carbon dioxide removal system where the carbon dioxide removal system is able to remove $75\,\%$ of the carbon dioxide from the stream entering the unit. The vapor stream leaving the CO_2 removal unit is split and $0.00318\,kmol/min$ is purged from the process and the remainder is combined with the remaining vapor stream (S28) that was not sent to the CO_2 removal unit. The combined recycle vapor stream (S33) is fed to the heat exchanger as the cold-side stream before mixing with ethylene feed stream. We define the gas streams that form a loop with the gas recycle stream (S34) as the gas loop of the process network.

In this process, one key safety constraint which needs to be taken into account is that the oxygen composition must be kept below $8\,mol\%$ throughout the gas loop to remain outside the explosive envelop of ethylene. In addition, several operation constraints must

be satisfied. The peak reactor temperature must stay below $200°C$ to avoid damage to the reactor catalyst. To avoid condensation in the reactor, the reactor inlet temperature must be greater than $130°C$. Since the process-to-process heat exchanger is designed to handle gas fluids, the heat exchanger hot fluid exit temperature must be greater than $130°C$. In addition, the liquid hold-ups must remain within the limits of 10 % to 90 % of allowable working liquid volume in the vessels.

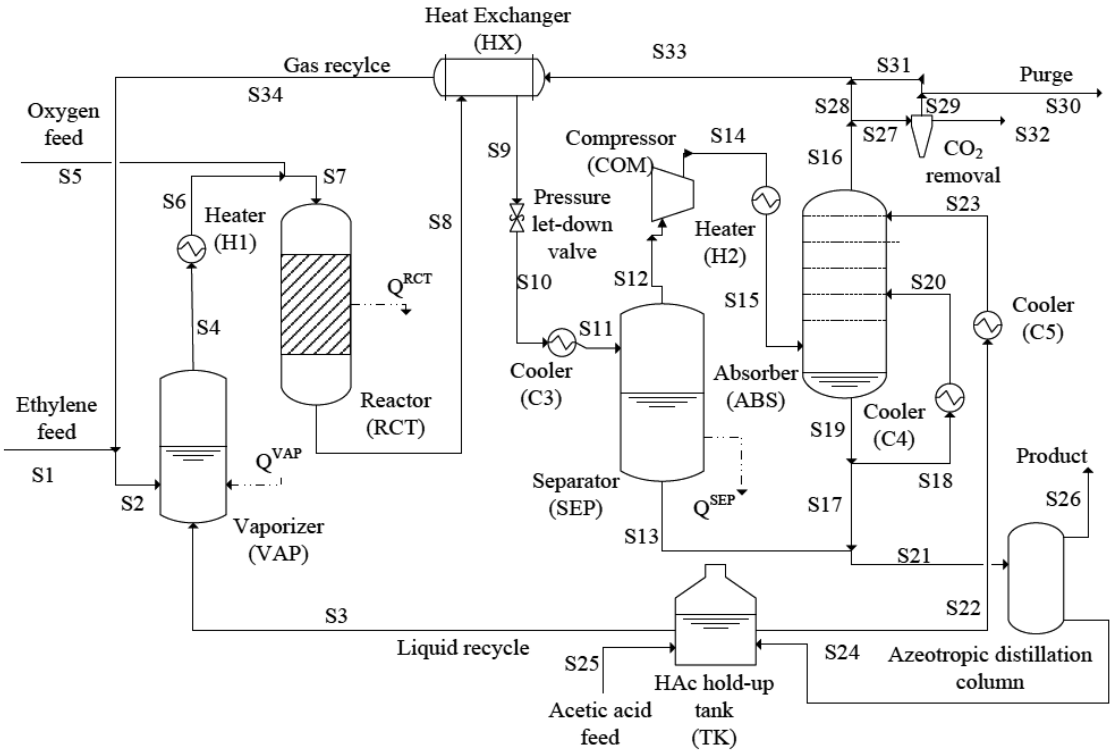

Figure 2.1: Process flow diagram of the vinyl acetate process network.

2.2 Thermodynamics and physical data

Ideal gas is assumed for the vapor phase. A standard Wilson liquid activity coefficient model is used to model the liquid phase with the Wilson parameters for each species pair *i*-*j* ($\tilde{a}_{ij}$) given in Table 2.1.

Table 2.1: Wilson parameters ($\tilde{a}_{ij}$) of each species pair existing in the liquid phase of the vinyl acetate process network taken from [22].

$\tilde{a}_{ij}$ $\left(\frac{kcal}{kmol}\right)$		i		
		VAc	H_2O	HAc
j	VAc	0	1384.6	-136.1
	H_2O	2266.4	0	670.7
	HAc	726.7	230.6	0

Pure component physical properties including molecular weight (MW_i), the liquid specific gravity (SpG_i), latent heat ($h_{L,i}$), liquid ($\bar{a}_i$ & $\bar{b}_i$) and vapor (a_i & b_i) heat capacity parameters of species i, $i = VAc$, H_2O, HAc, O_2, CO_2, C_2H_4, C_2H_6, and molar volume ($\tilde{v}_i$) are provided in Table 2.2.

Table 2.2: Physical properties of the species in the vinyl acetate process network taken from [5].

i	$M.W.$	SpG	h_{latent}	$\bar{a}$	$\bar{b}$	a	b	$\tilde{v}$
O_2	32	0.5	2300	0.3	0	0.218	0.0001	64.178
CO_2	44.01	1.18	2429	0.6	0	0.23	0	37.4
C_2H_4	28.052	0.57	1260	0.6	0	0.37	0.0007	49.347
C_2H_6	30.068	0.57	1260	0.6	0	0.37	0.0007	52.866
VAc	86.085	0.85	8600	0.44	0.0011	0.29	0.0006	101.564
H_2O	18.008	1.0	10684	0.99	0.0002	0.56	-0.0016	18.01
HAc	60.052	0.98	5486	0.46	0.0012	0.52	0.0007	61.455

The liquid specific gravity is determined based on the density of water at $0°C$. The temperature dependence on the vapor and liquid component constant pressure heat capacity is modeled as a linear dependence, as follows:

$$\hat{c}_i = (a_i + b_i T) MW_i \tag{2.1}$$

$$\check{c}_i = (\bar{a}_i + \bar{b}_i \bar{T}) MW_i \tag{2.2}$$

The temperature dependence on the vapor and liquid enthalpy is modeled as follows (i.e., $(\partial h_i / \partial T)_P = \hat{c}_i$):

$$h_i = (a_i T + 0.5 b_i T^2) MW_i + h_{L,i} \tag{2.3}$$

$$\bar{h}_i = (\bar{a}_i \bar{T} + 0.5 \bar{b}_i \bar{T}^2) MW_i \tag{2.4}$$

where h_i denotes the vapor enthalpy of species i and $\bar{h}_i$ denotes the liquid enthalpy of species i. The pressure dependence on heat capacity and enthalpy is assumed to be negligible. The Antoine equation is used to calculate the component saturated pressure (p_i^{sat}) in psia:

$$p_i^{sat} = \exp\left(\frac{\tilde{B}_i}{\tilde{C}_i + T(°C)} + \tilde{A}_i\right) \tag{2.5}$$

where the Antoine coefficients, $\tilde{A}_i$, $\tilde{B}_i$, $\tilde{C}_i$ are listed in Table 2.3.

Table 2.3: Component vapor pressure Antoine coefficients.

i	$\tilde{A}$	$\tilde{B}$	$\tilde{C}$
O_2	9.2	0	273
CO_2	7.937	0	273
C_2H_4	9.497	-313	273
C_2H_6	9.497	-313	273
VAc	12.6564	-2984.45	226.66
H_2O	14.6394	-3984.92	233.426
HAc	14.5236	-4457.83	258.45

2.3 Vaporizer

The vaporizer is assumed to be well mixed and vapor-liquid equilibrium is also assumed. Only the dynamics of the liquid phase in the vaporizer is taken into account. Vapor pressure and the vapor compositions are found using a bubble point calculation

$$P^{VAP}\check{y}_i^{VAP} = p_i^{sat,VAP}\gamma_i^{VAP}\check{x}_i^{VAP} \tag{2.6}$$

where γ_i^{VAP} represents the activity coefficient of species i in the liquid phase of the vaporizer. There are eight state variables in the vaporizer such as the liquid hold-up, the molar fractions, and the liquid temperature. The dynamic equations of the vaporizer are as follows:

$$\frac{d\bar{M}^{VAP}}{dt} = f_{S2} + \bar{f}_{S3} - f_{S4} \tag{2.7}$$

$$\frac{d\check{x}_i^{VAP}}{dt} = \frac{f_{S2}(\check{y}_{i,S2} - \check{x}_i^{VAP}) + \bar{f}_{S3}(\check{x}_{i,S3} - \check{x}_i^{VAP}) - f_{S4}(\check{y}_{i,S4} - \check{x}_i^{VAP})}{\bar{M}^{VAP}} \tag{2.8}$$

$$\frac{d\bar{T}^{VAP}}{dt} = \frac{f_{S2}(H_{S2} - \bar{H}^{VAP}) + \bar{f}_{S3}(\bar{H}_{S3} - \bar{H}^{VAP}) - f_{S4}(H_{S4} - \bar{H}^{VAP}) + Q^{VAP}}{\bar{M}^{VAP}\check{C}^{VAP}} \tag{2.9}$$

where $\bar{M}^{VAP}$ is the total number of moles in the liquid phase of the vaporizer, $\check{x}_i^{VAP}$ is the mole fraction of species i in the liquid phase of the vaporizer, and $\bar{T}^{VAP}$ is the temperature of the liquid phase of the vaporizer. The maximum allowable liquid volume in the vaporizer is $\bar{v}_{max}^{VAP} = 4\,m^3$.

2.4 Catalytic plug-flow reactor

A tubular packed-bed catalytic reactor is used to convert ethylene and acetic acid into the desired product, vinyl acetate. A combustion reaction also consumes ethylene in the reactor. The two reactions are given in Eq. 1.1. The reactor length is $10\,m$ and the diameter is $3.71\,cm$. It is assumed that the reactions only take place in the reactor. Plug flow through the reactor is assumed and thus, the temperature and concentration gradients are ignored in

the radial direction. In addition, diffusion is negligible in the axial direction. Temperature and concentration gradients from the bulk fluid to the external surface of the catalyst are negligible because mass and heat transfer are assumed to be very fast between phases. Mass flow rate per unit cross-sectional area is assumed to be constant. Catalyst deactivation is not considered so the catalyst activity is unity. The catalyst heat capacity Λ_{cat}, density ρ_{cat}, and porosity ϵ are $0.23\,kcal/kg^{\circ}C$, $385\,kg/m^3$, and 0.8, respectively. The dynamic model of the reactor is

$$\epsilon \frac{\partial c_i^{RCT}}{\partial t} = -\frac{\partial (c_i^{RCT} \check{v}^{RCT})}{\partial z} + \rho_{cat}(\zeta_{1,i} r_1 + \zeta_{2,i} r_2) \tag{2.10}$$

$$\begin{aligned}(\epsilon C^{RCT} \hat{C}^{RCT} + \rho_{cat}\Lambda_{cat}) \frac{\partial T^{RCT}}{\partial t} &= -\frac{\partial (\check{v}^{RCT} C^{RCT} \hat{C}^{RCT} T^{RCT})}{\partial z} \\ &\quad - \rho_{cat}(r_1 h_{rxn,1} + r_2 h_{rxn,2}) - q^{RCT}\end{aligned} \tag{2.11}$$

where C^{RCT} is the total vapor concentration, $\hat{C}^{RCT}$ is the vapor heat capacity, z is the axial coordinate along the length of the reactor ($z \in [0\,m, 10\,m]$), $\check{v}$ is the superficial velocity, and $\zeta_{1,i}$ and $\zeta_{2,i}$ are the stoichiometric coefficients for the reactions 1 and 2, respectively. To approximate the reactor dynamics of Eqs. 2.10-2.11, the reactor is modeled in ten sections in the axial direction ($l = 1, 2, \ldots, 10$), and the convective mass transfer and temperature gradients are assumed to have linear dependence in axial direction in each section:

$$\epsilon \frac{dc_{i,l}^{RCT}}{dt} = \frac{(c_{i,l-1}^{RCT} \check{v}_{l-1}^{RCT} - c_{i,l}^{RCT} \check{v}_l^{RCT})}{(z_l - z_{l-1})} + \rho_{cat}(\zeta_{1,i} r_{1,l} + \zeta_{2,i} r_{2,l}) \tag{2.12}$$

$$\begin{aligned}(\epsilon C_l^{RCT} \hat{C}_l^{RCT} + \rho_{cat}\Lambda_{cat}) \frac{dT_l^{RCT}}{dt} &= \frac{\check{v}_l^{RCT} C_l^{RCT} \hat{C}_l^{RCT} (T_{l-1}^{RCT} - T_l^{RCT})}{(z_l - z_{l-1})} \\ &\quad - \rho_{cat}(r_{1,l} h_{rxn,1} + r_{2,l} h_{rxn,2}) - q_l^{RCT}\end{aligned} \tag{2.13}$$

Since the Reynold's number of the packed bed reactor was estimated to be much greater than 1000, the pressure drop throughout the reactor was estimated to be less than 5% of the inlet pressure of the reactor using the Burke-Plummer equation [4, 3]. Furthermore, the pressure drop does not have a significant effect on the reaction rates as confirmed by extensive open-loop simulations of the reactor model. As a result, the pressure drop

throughout the reactor is not taken into account. The expressions of the chemical reaction rates [20] are

$$r_1 = 0.1036 \exp\left(\frac{-3674}{T(K)}\right) \frac{p_{O_2} p_{C_2H_4} p_{HAc}(1 + 1.7 p_{H_2O})}{(1 + 0.583 p_{O_2}(1 + 1.7 p_{H_2O}))(1 + 6.8 p_{HAc})} \tag{2.14}$$

$$r_2 = 1.9365 \times 10^5 \exp\left(\frac{-10,116}{T(K)}\right) \frac{p_{O_2}(1 + 0.68 p_{H_2O})}{(1 + 0.76 p_{O_2}(1 + 0.68 p_{H_2O}))} \tag{2.15}$$

where r_1 has units of moles of vinyl acetate produced per minute per gram of catalyst, and r_2 has units of moles of ethylene consumed per minute per gram of catalyst. Heat released per unit volume by the reactions (q_l^{RCT}) in l^{th} section is removed by water coolant on the shell side of the tubes and it is calculated by the following equation:

$$q_l^{RCT} = \bar{U}^{RCT}(T_l^{RCT} - T_{coolant}^{RCT}) \tag{2.16}$$

where $T_{coolant}^{RCT}$ is the water coolant temperature on the shell side which is assumed to be uniform and $\bar{U}^{RCT} = 269.84\, kcal/m^3 min^{\circ}C$ is the overall heat transfer coefficient per unit volume. There are 70 state variables in the reactor model such as fluid temperatures and concentrations of components for each section in the reactor.

2.5 Separator

It is assumed that the superheated hot effluent from the heat exchanger becomes saturated vapor through a pressure let-down valve. The saturated vapor is partially condensed through a cooler and then enters the separator. A temperature-pressure (TP) flash calculation, applicable when temperature and pressure are known since the equilibrium constant (K) mainly depends on temperature and pressure, is implemented to obtain the flow rates and compositions of the vapor (f_{S11} & $\check{y}_{S11}$) and liquid ($\bar{f}_{S11}$ & $\check{x}_{S11}$) streams entering the separator. The TP calculation sequence is implemented according to the following steps:

1. Guess the fraction of feed vaporized $\tilde{\alpha} := 0.62$ and the fraction of species i in S11 $\check{x}_{i,S11} := \check{x}_i^{SEP}$.

2. Calculate $K_{i,S11}$=$\frac{\gamma_{i,S11}(\check{x}_{i,S11},T_{S11})p^{sat}_{i,S11}(T_{S11})}{P^{SEP}}$.

3. Calculate $\check{x}_{i,S11} = \frac{\check{y}_{i,S10}}{(1+(K_{i,S11}-1)\tilde{\alpha})}$ and $\check{y}_{i,S11} = K_{i,S11}\check{x}_{i,S11}$.

4. Calculate $\psi = \sum_i (\check{x}_{i,S11} - \check{y}_{i,S11})$. If ψ is within an acceptable tolerance, STOP. Else, go to 5.

5. Update the fraction of feed vaporized: $\tilde{\alpha} := \tilde{\alpha} - 0.1\psi$ and go to step 2.

The number of moles and the pressure in the vapor phase are assumed to be constant while the change in the vapor temperature is assumed to exist because it is coupled with the change in the vapor mole fraction. Through extensive simulations, it is found that the change in temperature is insignificant even if mass accumulation and the pressure change of the vapor phase in the vessel are considered. Therefore, one could potentially neglect the change in the vapor temperature in the separator as well. Heat in the liquid phase is removed by a cooling jacket ($T^{SEP}_{coolant}$). There are 16 state variables such as liquid hold-up, molar fractions of components, and temperatures in the liquid phase and the vapor phase as well as the vapor phase pressure. These variables evolve according to the following dynamic equations:

$$\frac{d\bar{M}^{SEP}}{dt} = \bar{f}_{S11} - \bar{f}_{S13} \tag{2.17}$$

$$\frac{d\check{x}^{SEP}_i}{dt} = \frac{\bar{f}_{S11}(\check{x}_{S11,i} - \check{x}^{SEP}_i)}{(\bar{M}^{SEP})} \tag{2.18}$$

$$\frac{d\bar{T}^{SEP}}{dt} = \frac{\bar{f}_{S11}(\bar{H}_{S11} - \bar{H}^{SEP}) - UA^{SEP}(\bar{T}^{SEP} - T^{SEP}_{coolant})}{(\bar{M}^{SEP}\check{C}^{SEP})} \tag{2.19}$$

$$\frac{d\check{y}^{SEP}_i}{dt} = \frac{f_{S11}(\check{y}_{S11,i} - \check{y}^{SEP}_i)}{(M^{SEP})} \tag{2.20}$$

$$\frac{dT^{SEP}}{dt} = \frac{f_{S11}(H_{S11} - H^{SEP})}{(M^{SEP}\hat{C}^{SEP})} \tag{2.21}$$

The maximum allowable liquid volume in the separator is $\bar{v}^{SEP}_{max} = 8\,m^3$.

2.6 Absorber

The purpose of the absorber is to recover the remaining vinyl acetate from the vapor effluent that leaves the separator. The gas absorber consists of eight theoretical stages ($l = 1, 2, ..., 8$) and a liquid hold-up base. It is assumed that there is no chemical reaction taking place at each stage, and the absorber pressure which is determined by the exit pressure of the compressor is uniform throughout the absorber. A mass transfer rate-based model is implemented to describe the mass transfer and heat transfer between the liquid phase and the vapor phase at each stage; vapor-liquid equilibrium is assumed to exist at the interface in the rate-based model. The liquid hold-up at each stage is assumed to be well mixed.

For convective flow, the mass transfer coefficient is a function of flow rate, temperature, and pressure. The mass transfer coefficient in this model, nevertheless, is assumed to be constant at each stage. For this reason, the mass transfer rate calculated from the model for a component at each stage might exceed the total mass of the component in the bulk phase. Thus, the maximum mass transfer rate for a component is assumed to be constrained by half the amount in the bulk phase. The convective mass coefficient (k) is 27.22 $kmol/min$. The individual component mass transfer rate ($N_{i,l}^{ABS}$) between two phases at each stage is determined by the following equation:

$$N_{i,l}^{ABS} = \min\left\{\left|k(\check{y}_{i,(l-1)}^{ABS} - \check{y}_{i,l}^{int})\right|, 0.5 f_{(l-1)}^{ABS}\check{y}_{i,(l-1)}^{ABS}\right\}, \begin{cases} n_{i,l}^{ABS} = N_{i,l}^{ABS}, \text{ if } \check{y}_{i,(l-1)}^{ABS} > \check{y}_{i,l}^{int} \\ n_{i,l}^{ABS} = -N_{i,l}^{ABS}, \text{ if } \check{y}_{i,(l-1)}^{ABS} < \check{y}_{i,l}^{int} \end{cases} \tag{2.22}$$

The vapor compositions of species i ($\check{y}_{i,l}^{int}$) at the interface of the l^{th} theoretical stage is obtained using an equilibrium calculation. Two forms of energy transfer occur between the two phases at each stage: conductive heat transfer due to temperature gradients and convective heat transfer due to the transferring components. Conductive heat transfer (Q_l^{ABS}) and convective heat transfer ($Q_{tr,l}^{ABS}$) from the vapor phase to the liquid phase at

l^{th} stage are calculated based on the following equations:

$$Q_l^{ABS} = UA_l^{ABS}(T_{(l-1)}^{ABS} - \bar{T}_l{}^{ABS}) \tag{2.23}$$

$$Q_{tr,l}^{ABS} = \sum_{i=1}^{7} n_{i,l}^{ABS} h_{i,l}^{ABS}(\bar{T}) \tag{2.24}$$

where the overall heat transfer coefficient $UA_l^{ABS} = 100.8\ kcal/kmol$ for $l = 1,\ 2$ and $UA_l^{ABS} = 50.4\ kcal/kmol$ for $l = 3,\ 4, \ldots, 8$. The absorber is divided into two sections. The bottom section contains two stages and the base. The top section contains six stages. The base has an inlet stream from the first stage and an outlet stream which is split into a circulation stream ($\bar{f}_{S20}$) and a stream ($\bar{f}_{S17}$) used to regulate the liquid hold-up of the base. The dynamics of the base is described as follows:

$$\frac{d\bar{M}_b^{ABS}}{dt} = \bar{f}_1^{ABS} - \bar{f}_{S17} - \bar{f}_{S20}, \tag{2.25}$$

$$\frac{d\check{x}_{i,b}^{ABS}}{dt} = \frac{\bar{f}_1^{ABS}(\check{x}_{i,1}^{ABS} - \check{x}_{i,b}^{ABS})}{\bar{M}_b^{ABS}} \tag{2.26}$$

$$\frac{d\bar{T}_b^{ABS}}{dt} = \frac{\bar{f}_1^{ABS}(\bar{H}_1^{ABS} - \bar{H}_b^{ABS})}{\bar{M}_b^{ABS}\check{C}_b{}^{ABS}} \tag{2.27}$$

where the subscript b denotes the base. A cooled circulation stream is fed to the second stage ($l = 2$) for an initial gas scrubbing. The dynamics of the second stage is described as follows:

$$\frac{d\bar{M}_l^{ABS}}{dt} = (\bar{f}_{l+1}^{ABS} + \bar{f}_{S20} + \bar{n}_{net,l}^{ABS} - \bar{f}_l^{ABS}) \tag{2.28}$$

$$\frac{d\check{x}_{i,l}^{ABS}}{dt} = \frac{\bar{f}_{l+1}^{ABS}(\check{x}_{i,(l+1)}^{ABS} - \check{x}_{i,l}^{ABS}) + \bar{f}_{S20}(\check{x}_{i,b}^{ABS} - \check{x}_{i,l}^{ABS}) + n_{i,l}^{ABS} - \bar{n}_{net,l}^{ABS}\check{x}_{i,l}^{ABS}}{\bar{M}_l^{ABS}} \tag{2.29}$$

$$\frac{d\bar{T}_l^{ABS}}{dt} = \frac{\bar{f}_{l+1}^{ABS}(\bar{H}_{l+1}^{ABS} - \bar{H}_l^{ABS}) + \bar{f}_{S20}(\bar{H}_{S20}^{ABS} - \bar{H}_l^{ABS}) + Q_{tr,l}^{ABS} + Q_l^{ABS} - \bar{n}_{net,l}^{ABS}\bar{H}_l^{ABS}}{\bar{M}_l^{ABS}\check{C}_l{}^{ABS}} \tag{2.30}$$

where $\bar{n}_{net,l}$ is the net amount of material transferring to the liquid phase as shown below:

$$\bar{n}_{net,l}^{ABS} = \sum_{i=1}^{7} n_{i,l}^{ABS} \tag{2.31}$$

For stages (l =1, 3, 4, 5, 6, and 7), there are an inlet liquid stream from the above stage and an outlet liquid stream which leaves the stage. The dynamics of these stages are described

by the following equations:

$$\frac{d\bar{M}_l^{ABS}}{dt} = (\bar{f}_{l+1}^{ABS} + \bar{n}_{net,l}^{ABS} - \bar{f}_l^{ABS}) \tag{2.32a}$$

$$\frac{d\check{x}_{i,l}^{ABS}}{dt} = \frac{\bar{f}_{l+1}^{ABS}(\check{x}_{i,(l+1)}^{ABS} - \check{x}_{i,l}^{ABS}) + n_{i,l}^{ABS} - \bar{n}_{net,l}^{ABS}\check{x}_{i,l}^{ABS}}{\bar{M}_l^{ABS}} \tag{2.32b}$$

$$\frac{d\bar{T}_l^{ABS}}{dt} = \frac{\bar{f}_{l+1}^{ABS}(\bar{H}_{l+1}^{ABS} - \bar{H}_l^{ABS}) + Q_{tr,l}^{ABS} + Q_l^{ABS} - \bar{n}_{net,l}^{ABS}\bar{H}_l^{ABS}}{\bar{M}_l^{ABS}\check{C}_l^{ABS}} \tag{2.32c}$$

A liquid stream ($\bar{f}_{S23}$) from the acetic acid hold-up tank which is cooled and enters the last stage ($l = 8$) serves as final gas scrubbing stream. The dynamics of the last stage are described by the following equations:

$$\frac{d\bar{M}_l^{ABS}}{dt} = (\bar{f}_{S23} + \bar{n}_{net,l}^{ABS} - \bar{f}_l^{ABS}) \tag{2.33a}$$

$$\frac{d\check{x}_{i,l}^{ABS}}{dt} = \frac{\bar{f}_{S23}(\check{x}_{i,S23} - \check{x}_{i,l}^{ABS}) + n_{i,l}^{ABS} - \bar{n}_{net,l}^{ABS}\check{x}_{i,l}^{ABS}}{\bar{M}_l^{ABS}} \tag{2.33b}$$

$$\frac{d\bar{T}_l^{ABS}}{dt} = \frac{\bar{f}_{S23}(\bar{H}_{S23} - \bar{H}_l{}^{ABS}) + Q_{tr,l}^{ABS} + Q_l^{ABS} - \bar{n}_{net,l}^{ABS}\bar{H}_l^{ABS}}{\bar{M}_l^{ABS}\check{C}_l{}^{ABS}} \tag{2.33c}$$

Since only liquid phase dynamics is considered, the mass flow rate, the compositions, and the temperature of an exit vapor stream from each stage are calculated using steady-state mass, component, and energy balances around the vapor phase at each stage. There are a total of 72 state variables including the liquid hold-up, the compositions and the liquid temperature at each stage and at the base. The maximum allowable liquid volume in the absorber is $\bar{v}_{max}^{ABS} = 8.5\,m^3$.

2.7 Acetic acid hold-up tank

The acetic acid tank is used to mix the bottom product stream from the azeotrope distillation column and the HAc feed stream. The acetic acid hold-up tank allows for a better control of the liquid recycle loop to prevent the snowballing effect. There are four state variables, which are the liquid hold-up, molar fractions of VAc and HAc, and the liquid

temperature. The dynamic equations are as follows:

$$\frac{d\bar{M}^{TK}}{dt} = (\bar{f}_{S24} + \bar{f}_{S25} - \bar{f}_{S3} - \bar{f}_{S22}) \tag{2.34}$$

$$\frac{d\check{x}_i^{TK}}{dt} = \frac{\bar{f}_{S24}(\check{x}_{i,S24} - \check{x}_i^{TK}) + \bar{f}_{S25}(\check{x}_{i,S25} - \check{x}_i^{TK})}{\bar{M}^{TK}} \tag{2.35}$$

$$\frac{d\bar{T}^{TK}}{dt} = \frac{\bar{f}_{S24}(\bar{H}_{S24} - \bar{H}^{TK}) + \bar{f}_{S25}(\bar{H}_{S25} - \bar{H}^{TK})}{\bar{M}^{TK}\check{C}^{TK}} \tag{2.36}$$

The maximum allowable liquid volume in the tank is $\bar{v}_{max}^{TK} = 2.83\,m^3$.

2.8 Compressor, heat exchanger, heaters and coolers

The dynamics of the compressor, heat exchanger, heaters and coolers are assumed to be adequately represented by first-order systems of the form:

$$\frac{dx}{dt} = \frac{\bar{x}_s - x}{\tau} \tag{2.37}$$

where $\bar{x}_s$ is the steady-state computed by the steady-state energy balance, x is a state variable, and τ is a time constant.

Compressor

Isentropic compression is assumed to calculate the outlet temperature and pressure of the compressor. The actual work input (W_s^{COM}) to the compressor is a manipulated input. The mean specific heat capacity [32] ($\hat{C}_{mean}^{COM}$) is used and assumed to be linearly dependent on the log-mean temperature of the inlet and outlet stream. Two state variables are present in the compressor: the outlet temperature and the pressure. It is assumed that a five-minute time constant can be used to describe the dynamics of the compressor.

Heat exchanger

The NTU-Effectiveness method [11] based on the single-tube heat exchanger with counter-flow is used to calculate the steady-state heat exchanger exit temperature. The overall heat

transfer coefficient (UA^{HX}) [5] is correlated according to the nominal overall heat transfer coefficient, and the ratio of the stream flow rates to the nominal flow rates to the power of 0.8, as follows:

$$UA^{HX} = \frac{UA_{ref}}{2}\left(\left(\frac{f_{S32}MW_{S32}}{m_{cold,ref}}\right)^{0.8} + \left(\frac{f_{S9}MW_{S9}}{m_{hot,ref}}\right)^{0.8}\right) \tag{2.38}$$

where the reference overall heat transfer coefficient is $UA_{ref} = 113.33\,kcal/min°C$, the reference cold stream flow rate is $m_{cold,ref} = 498.952\,kg/min$ and the reference hot stream flow rate is $m_{hot,ref} = 589.67\,kg/min$. The exit temperatures for the cold stream and the hot stream are the two state variables in the heat exchanger. A five-minute time constant is introduced to describe the dynamics.

Coolers and heaters

There are three coolers and two heaters in the process. A two-minute time constant is used to describe their dynamics. The exit temperature is a state variable and the heat input is a manipulated input in each of these units.

2.9 Nonlinear dynamic model of the vinyl acetate process

The nonlinear dynamic model of the vinyl acetate consists of 179 ODEs, 351 algebraic equations, and 23 inequality process constraints. The process constraints include the liquid hold-up volume in vessels, the oxygen composition in the gas loop, the inlet temperature of the reactor, the temperature in the reactor, the hot-side outlet temperature of the heat exchanger, and the pressure drop in the gas loop. In short, the nonlinear dynamic model of the vinyl acetate process network can be described by the following state-space model:

$$\dot{x}(t) = f(x(t), u_1(t), \ldots, u_{20}(t)) \tag{2.39a}$$

$$0 = g(x(t), u_1(t), \ldots, u_{20}(t)) \tag{2.39b}$$

$$0 \leq h(x(t), u_1(t), \ldots, u_{20}(t)) \tag{2.39c}$$

where $x(t) \in R^{n_x}$ denotes the vector of state variables of the system and $u_i(t) \in R$, $i = 1, \ldots, 20$ denotes the i^{th} control (manipulated) input, respectively. In the nonlinear model of Eq. 2.39, the vector function f is the right-hand-side of the nonlinear dynamic equations, the vector function g is the family of algebraic equations, and the vector function h is the family of process constraints which may depend on states and inputs. In this process, there are 20 available inputs which are shown in Table 2.4 along with the available range for each input and steady-state values u_s. The steady-state that corresponds to the steady-state input u_s is denoted as x_s. We note that in our model seven of the inputs are fixed to specific values.

Table 2.4: Input constraints and steady-state values.

Manipulated Input (u)	Loop	Input Number	Range	Steady-state (u_s)	Unit
Q^{H1}	MPC	1	0-50000	5078.69	$\frac{kcal}{min}$
Q^{H2}	MPC	2	-10000-50000	1461.14	$\frac{kcal}{min}$
Q^{C3}	MPC	3	0-30000	15491.57	$\frac{kcal}{min}$
Q^{C4}	MPC	4	0-30000	7250.42	$\frac{kcal}{min}$
Q^{C5}	MPC	5	0-5000	1881.2	$\frac{kcal}{min}$
f_{S4}	PI	6	8-15	12.113916	$\frac{kmol}{min}$
f_{S5}	PI	7	0-2.268	0.47744	$\frac{kmol}{min}$
$\bar{f}_{S13}$	PI	8	0-8	2.73964	$\frac{kmol}{min}$
$\bar{f}_{S17}$	PI	9	0-4.536	1.20871	$\frac{kmol}{min}$
$\bar{f}_{S25}$	PI	10	0-4.536	0.74435	$\frac{kmol}{min}$
Q^{VAP}	PI	11	0-143340	16933.247	$\frac{kcal}{min}$
$T^{RCT}_{coolant}$	PI	12	110-150	133.46	$^{\circ}C$
W^{COM}_{s}	PI	13	0-1000	275.64	$\frac{kcal}{kmol}$
$T^{SEP}_{coolant}$	Fixed	14	0-80	37.72	$^{\circ}C$
f_{S1}	Fixed	15	0-7.56	0.905	$\frac{kmol}{min}$
$\bar{f}_{S18}$	Fixed	16	0-50	15.35	$\frac{kmol}{min}$
$\bar{f}_{S22}$	Fixed	17	0-7.56	0.8125	$\frac{kmol}{min}$
$\bar{f}_{S3}$	Fixed	18	0-4.536	2.1924	$\frac{kmol}{min}$
f_{S27}	Fixed	19	0-22.68	6.556	$\frac{kmol}{min}$
f_{S30}	Fixed	20	0-0.02268	0.00318	$\frac{kmol}{min}$

Chapter 3

Model predictive control formulations

3.1 Notation

The operator $|\cdot|$ is used to denote the Euclidean norm of a vector. The symbol Ω_r is used to denote the set $\Omega_r := \{x \in R^{n_x} : V(x) \leq r\}$ where V is a scalar function. The symbol diag(v) denotes a matrix whose diagonal elements are the elements of a vector v and all the other elements are zeros. The superscript v^T denotes the transpose of a vector v.

3.2 Economic measure

In this work, we aim to maximize the overall vinyl acetate production in the azeotropic distillation overhead stream (S26) so an economic measure is chosen to account for the reaction selectivity in the reactor and the separation quality in the separator and the absorber as follows:

$$L(x,u) = A_1 \frac{c^{RCT}_{VAc,10}}{c^{RCT}_{CO_2,10}} + A_2 \check{x}^{SEP}_{VAc} + A_3 \check{x}^{ABS}_{VAc,b} \tag{3.1}$$

where $L(x,u)$ is the economic measure, $A := [A_1\ A_2\ A_3] = [30\ 1000\ 1000]$ are the constant weighting coefficients which are chosen such that each term in the economic measure is of

the same order of magnitude, $c^{RCT}_{VAc,10}$ and $c^{RCT}_{CO_2,10}$ are the VAc and CO_2 concentrations at the 10^{th} section of the reactor, and $\check{x}^{SEP}_{VAc}$ and $\check{x}^{ABS}_{VAc,b}$ are the vinyl acetate liquid molar fractions in the separator and the absorber base, respectively. The first term of the measure describes reaction selectivity of VAc with respect to CO_2 in the reactor. The second term and the third term account for VAc recovery in the separator and the absorber.

Remark 1 *In this work, the weighting coefficients have been chosen such that each term in the economic cost is significant. In practice, these coefficients would be chosen based on process objectives, operating costs, and material prices.*

3.3 Controller synthesis

In the process network, the heater ($H1$) prior to the reactor affects the inlet stream temperature which, in turn, affects the reaction rates and the reaction selectivity. The cooler ($C3$) prior to the separator determines the quality of flashing streams. The heater ($H2$) prior to the absorber and the side coolers ($C4$) and ($C5$) account for the VAc recovery. Hence, these five inputs have direct influence on the economic measure and on closed-loop economic performance. Therefore, we propose a control architecture which comprises of LMPC or LEMPC regulating the inputs of the heaters and coolers, a set of eight independent PI controllers regulating eight inputs to maintain closed-loop stability, and seven inputs that are fixed. Figure 3.1 shows the control architecture. A summary of which manipulated inputs are controlled by MPC or PI or are fixed along with the available control energy for each manipulated input and steady-state values u_s are given in Table 2.4.

In this work, we assume that the full system state x is measured at every sampling period ($\tilde{\Delta}$). State measurements are sent to the PI controllers at synchronous time instants $t_q = q\Delta_{PI}$, $q = 0, 1, \ldots$ and sent to the LMPC or LEMPC at synchronous time instants $t_k = k\Delta$, $k = 0, 1, \ldots$. Taking into account closed-loop stability consideration, the sampling times for the LMPC/LEMPC and the set of PI controllers are chosen to be $\Delta_{PI} = \tilde{\Delta}$ and

$\Delta = 10\tilde{\Delta}$, respectively, where $\tilde{\Delta} = 0.001$ minutes. The manipulated input vector computed by the PI controllers can be expressed as follows:

$$u_{PI,i} = K_{c,i}(\eta_i - \eta_i^{set}) + \frac{K_{c,i}}{\tau_{I,i}} \int_0^t (\eta_i - \eta_i^{set})\, dt' + u_{s,i},\ i = 6, \ldots, 13 \tag{3.2}$$

where u_{PI} is the vector of manipulated inputs on the set of PI controllers given by $u_{PI}^T = [u_{PI,6}\, u_{PI,7}$

$\cdots\ u_{PI,13}] = [f_{S4}\, f_{S5}\, \bar{f}_{S13}\, \bar{f}_{S17}\, \bar{f}_{S25}\, Q^{VAP}\, T_{coolant}^{RCT}\, W_s^{COM}]$, η is the vector of the controlled outputs given by $\eta^T = [\bar{v}^{VAP}\, \check{x}_{O_2,1}^{RCT}\, \bar{v}^{SEP}\, \bar{v}^{ABS}\, \bar{v}^{TK}\, \bar{T}^{VAP}\, T_{10}^{RCT}\, P^{COMP}]$, η^{set} is the set-point vector, K_c is the vector of the proportional gains, $K_c = [K_{c6}\, K_{c7}\ \cdots\ K_{c13}]$ and τ_I is the vector of the integral time constants, $\tau_I = [\tau_{I6}\, \tau_{I7}\ \cdots\ \tau_{I13}]$. Several closed-loop simulations were completed to tune the proportional-integral controllers. Closed-loop simulations were initially performed under proportional control loops tuned to provide sufficiently small rise times and no oscillation in the controlled outputs. Subsequently, integral action was added to eliminate the residual steady-state errors. For example, the proportional gain and integral time constant for the PI controller that regulates oxygen feed flow rate were chosen to avoid excessive overshoot such that the oxygen concentration in the gas loop is kept outside the explosive region. The proportional gains (K_c), integration time constants (τ_I), and set-points (η^{set}) for PI controllers are:

$$K_c^T = (10^2) \cdot [1\ 0.1\ 1\ 1\ 1\ 75\ 0.3\ 500]$$

$$\tau_I^T = [80\ 0.1\ 350\ 200\ 50\ 40\ 4.5\ 50]$$

$$(\eta^{set})^T = [2.72\ 0.01256\ 4\ 4.25\ 1.415\ 120\ 158.5\ 128]$$

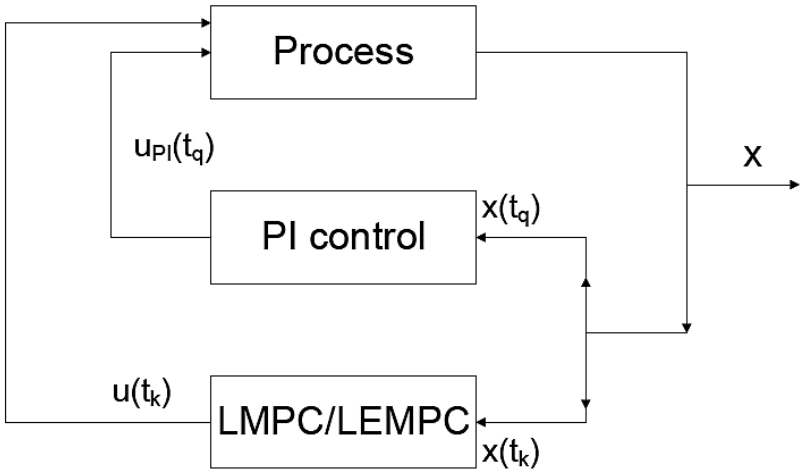

Figure 3.1: The control architecture designed for the vinyl acetate process network.

3.4 Lyapunov-based controller

In the LMPC and LEMPC designs proposed in the literature [27, 13], the nonlinear system is assumed to be stabilizable by assuming the existence of a Lyapunov-based controller $\hat{h}(x)^T = [\hat{h}_1(x) \ \cdots$

$\hat{h}_m(x)]$ that can render the steady-state of the nonlinear system asymptotically stable under continuous implementation while satisfying the input constraints for all the states x inside a given stability region. The Lyapunov-based controller ($\hat{h}(x)$) used for the vinyl acetate process network is another set of PI controllers, namely,

$$\hat{h}(x)^T = \hat{u}_{PI}^T = [\hat{u}_{PI,1} \cdots \hat{u}_{PI,5}] \tag{3.3}$$

where $\hat{u}_{PI}$ uses the formulation of Eq. 3.2, $\hat{u}_{PI}^T = [Q^{H1} \, Q^{H2} \, Q^{C3} \, Q^{C4} \, Q^{C5}]$ and the set-point vector $(\hat{\eta}^{set})^T = [T^{H1,set} \, T^{H2,set} \, T^{C3,set} \, \bar{T}^{C4,set} \, \bar{T}^{C5,set}]$. The input constraints and the steady-state input values are listed in Table 2.4. Closed-loop simulations of the vinyl acetate process network confirmed that the Lyapunov-based controller along with other

control inputs either on PI controllers or fixed values can regulate the process to the steady-state. The proportional gains ($\hat{K}_c$), integration time constant ($\hat{\tau}_I$), and set-points ($\hat{\eta}^{set}$) for the Lyapunov-based controllers are:

$$\hat{K}_c^T = (10^2) \cdot [2.5\ 30\ 10\ 50\ 5]$$

$$\hat{\tau}_I^T = [80\ 220\ 7.14\ 90\ 50\ 52.6]$$

$$(\hat{\eta}^{set})^T = [145\ 83\ 47\ 32.5\ 40]$$

Using converse Lyapunov theorems [6, 19], this stabilizability property implies that there exist a continuously differentiable Lyapunov function $V(x)$ for the nominal closed-loop system in R^{n_x}. We denote the region $\Omega_\rho \subseteq O$ as the stability region of the closed-loop system under the Lyapunov-based controller $\hat{h}(x)$. In the vinyl acetate process network, we use a quadratic Lyapunov function of the form

$$V(x) = (x - x_s)^T \hat{P} (x - x_s) \tag{3.4}$$

for the design of the LMPC and LEMPC where $\hat{P} \in R^{n_x} \times R^{n_x}$ is a positive definite diagonal matrix and x_s is the steady-state. The diagonal elements of $\hat{P}$ were chosen based on the magnitude of the vector field f of Eq. 2.39a of the closed-loop system with inputs $1, \ldots, 13$ on PI controllers (i.e., both the controllers u_{PI} and $\hat{h}(x)$ applied to the process network). Specifically, if the magnitude of the ith element of the vector field f was consistently positive or negative, the diagonal element $\hat{p}_{ii}$ of the matrix $\hat{P}$ was increased. The final $\hat{P}$ was selected through extensive simulations such that the PI controllers decreased the Lyapunov function over each sampling period when the PI controllers are implemented in a sample-and-hold fashion and when the process network is initialized at an off-steady-state initial condition. The weights in $\hat{P}$ matrix and the corresponding states are listed in Table 3.1.

Remark 2 *Explicit stabilizing control laws that provide explicitly defined regions of attraction for the closed-loop system have been developed using Lyapunov techniques for various classes of nonlinear systems; the reader may refer to refs [6, 8, 17, 18] for results in this area.*

Remark 3 *We note that the Lyapunov-based controller is typically formulated as a static controller as in refs [27, 26]. Even though PI controllers are dynamic controllers, the set of PI controllers with little integral action can be considered as a Lyapunov-based controller as long as the independent PI control loops can stabilize the process network.*

Table 3.1: Weights in $\hat{P}$ matrix.

$Weights$	$States(x)$
1	$\bar{T}_1^{ABS}$, $\bar{T}_2^{ABS}$, $\bar{T}_5^{ABS}$, $\bar{T}_6^{ABS}$, T^{COMP}
10	$\check{x}_{HAC}^{VAP}$, $\check{x}_{VAc}^{SEP}$, $\check{x}_{H_2O}^{SEP}$, $\check{x}_{HAc}^{SEP}$, $\check{x}_{VAc,b}^{ABS}$, $\check{x}_{H_2O,b}^{ABS}$, $\check{x}_{HAc,b}^{ABS}$, $\check{x}_{VAc,1}^{ABS}$, $\check{x}_{H_2O,1}^{ABS}$, $\check{x}_{VAc,2}^{ABS}$ $\check{x}_{H_2O,2}^{ABS}$, $\check{x}_{H_2O,3}^{ABS}$, $\check{x}_{HAc,l}^{ABS}$, $\check{x}_{HAc}^{TK}$, $\check{y}_{C_2H_4}^{SEP}$, T^{SEP}, $\bar{T}^{SEP}$, $\bar{T}^{VAP}$, T_l^{RCT}, $\bar{T}_3^{ABS}$ $\bar{T}_4^{ABS}$, $\bar{T}_7^{ABS}$, $\bar{T}_8^{ABS}$, $\bar{T}_b^{ABS}$, $\bar{T}^{TK}$, T^{H1}, T^{H2}, T^{C3}, T^{C4}, T^{C5}, T_{S34}, T_{S9} $\bar{M}_l^{ABS}$, $\bar{M}_b^{ABS}$, $\bar{M}^{SEP}$, $\bar{M}^{VAP}$, $\bar{M}^{TK}$, P^{SEP}, P^{COMP}, $c_{C_2H_4,l}^{RCT}$
100	$\check{x}_{C_2H_4}^{VAP}$, $\check{x}_{H_2O}^{VAP}$, $\check{x}_{C_2H_4}^{SEP}$, $\check{x}_{VAc,5}^{ABS}$, $\check{x}_{VAc,6}^{ABS}$, $\check{x}_{H_2O,4}^{ABS}$, $\check{x}_{H_2O,5}^{ABS}$, $\check{x}_{H_2O,6}^{ABS}$, $\check{x}_{H_2O,7}^{ABS}$ $\check{x}_{VAc,3}^{ABS}$, $\check{x}_{VAc,4}^{ABS}$, $\check{x}_{H_2O,8}^{ABS}$, $\check{x}_{b,C_2H_4}^{ABS}$, $\check{x}_{C_2H_4,l}^{ABS}$, $\check{y}_{VAc}^{SEP}$, $\check{y}_{H_2O}^{SEP}$, $\check{y}_{O_2}^{SEP}$, $\check{y}_{CO_2}^{SEP}$ $c_{O_2,3}^{RCT}$, $c_{O_2,4}^{RCT}$, $c_{O_2,5}^{RCT}$, $c_{VAc,10}^{RCT}$, $c_{H_2O,8}^{RCT}$, $c_{H_2O,9}^{RCT}$, $c_{H_2O,10}^{RCT}$, $c_{O_2,1}^{RCT}$, $c_{O_2,2}^{RCT}$, $c_{HAc,l}^{RCT}$
1000	$\check{x}_{O_2}^{SEP}$, $\check{x}_{O_2,1}^{ABS}$, $\check{x}_{O_2,2}^{ABS}$, $\check{x}_{VAc,7}^{ABS}$, $\check{x}_{VAc,8}^{ABS}$, $\check{x}_{O_2,b}^{ABS}$, $\check{y}_{HAc}^{SEP}$, $c_{O_2,6}^{RCT}$, $c_{O_2,7}^{RCT}$, $c_{O_2,8}^{RCT}$ $c_{O_2,9}^{RCT}$, $c_{O_2,10}^{RCT}$, $c_{VAc,2}^{RCT}$, $c_{VAc,3}^{RCT}$, $c_{VAc,4}^{RCT}$, $c_{VAc,5}^{RCT}$, $c_{VAc,6}^{RCT}$, $c_{VAc,7}^{RCT}$, $c_{VAc,8}^{RCT}$ $c_{VAc,9}^{RCT}$, $c_{H_2O,1}^{RCT}$, $c_{H_2O,2}^{RCT}$, $c_{H_2O,3}^{RCT}$, $c_{H_2O,4}^{RCT}$, $c_{H_2O,5}^{RCT}$, $c_{H_2O,6}^{RCT}$, $c_{H_2O,7}^{RCT}$, $c_{CO_2,l}^{RCT}$
10000	$\check{x}_{O_2}^{VAP}$, $\check{x}_{CO_2}^{VAP}$, $\check{x}_{VAc}^{VAP}$, $\check{x}_{C_2H_4}^{SEP}$, $\check{x}_{O_2,3}^{ABS}$, $\check{x}_{O_2,4}^{ABS}$, $\check{x}_{O_2,5}^{ABS}$ $\check{x}_{O_2,6}^{ABS}$, $\check{x}_{O_2,7}^{ABS}$, $\check{x}_{O_2,8}^{ABS}$, $\check{x}_{b,CO_2}^{ABS}$, $\check{x}_{CO_2,l}^{ABS}$, $c_{VAc,1}^{RCT}$
100000	$\check{x}_{VAc}^{TK}$

3.5 Lyapunov-based model predictive control

LMPC is capable of computing optimal control inputs while accounting for input and state constraints and ensuring the stability of the closed-loop system. The LMPC design follows the formulation of our previous works [27, 26] and takes in account the nonlinear system of Eq. 2.39 (where, without any loss of generality, $x_s = 0$ is the stabilizing steady-state), as

follows:

$$\min_{u_1,\ldots,u_5\in S(\Delta)} \int_{t_k}^{t_{k+N}} [\tilde{x}^T(\tilde{\tau})\check{Q}_c\tilde{x}(\tilde{\tau}) + u^T(\tilde{\tau})\check{R}_c u(\tilde{\tau})]d\tilde{\tau} \tag{3.5a}$$

$$\text{s.t. } \dot{\tilde{x}}(t) = f(\tilde{x}(t), u_1(t), \ldots, u_{20}(t)) \tag{3.5b}$$

$$0 = g(\tilde{x}(t), u_1(t), \ldots, u_{20}(t)),\ \forall\, t \in [t_k, t_{k+N}) \tag{3.5c}$$

$$0 \leq h(\tilde{x}(t), u_1(t), \ldots, u_{20}(t)),\ \forall\, t \in [t_k, t_{k+N}) \tag{3.5d}$$

$$u_i(t) \in U_i,\ i = 1, \ldots, 13,\ \forall\, t \in [t_k, t_{k+N}) \tag{3.5e}$$

$$u_i(t) = u_{PI,i}(t),\ i = 6, \ldots, 13,\ \forall\, t \in [t_k, t_{k+N}) \tag{3.5f}$$

$$u_i(t) = u_i^{fixed},\ i = 14, \ldots, 20,\ \forall\, t \in [t_k, t_{k+N}) \tag{3.5g}$$

$$\tilde{x}(t_k) = x(t_k) \tag{3.5h}$$

$$\begin{aligned}\frac{\partial V(x)}{\partial x} f(x(t_k), u_1(t_k), \ldots, u_5(t_k), u_{PI,6}(t_k), \ldots, u_{PI,13}(t_k), u_{14}^{fixed}, \ldots, u_{20}^{fixed}) \\ \leq \frac{\partial V(x)}{\partial x} f(x(t_k), \hat{h}_1(x(t_k)), \ldots, \hat{h}_5(x(t_k)), u_{PI,6}(t_k), \ldots, u_{PI,13}(t_k), \\ u_{14}^{fixed}, \ldots, u_{20}^{fixed})\end{aligned} \tag{3.5i}$$

where $S(\Delta)$ is the family of piece-wise constant functions with sampling time Δ, N is the prediction horizon, $\check{Q}_c$ and $\check{R}_c$ are strictly positive definite weight matrices, $\tilde{x}$ is the predicted state trajectory of the nominal system with inputs $1, \ldots, 5$ computed by the LMPC, $6, \ldots, 13$ computed by the PI controllers, and fixed inputs u_i^{fixed} for inputs $14, \ldots, 20$, and initial state $x(t_k)$. The weighting matrices $\check{Q}_c$ and $\check{R}_c$ are listed in the Appendix.

The optimal solution to this optimization problem is denoted by $u_i^*(\tilde{\tau}|t_k),\ i = 1, ..., 5$, which is defined for $\tilde{\tau} \in [t_k, t_{k+N})$. The LMPC is implemented in a receding horizon fashion; namely, the optimization problem of Eq. 3.5 is solved along the prediction horizon at each sampling time and $u_i^*(t|t_k),\ i = 1, ..., 5$ are applied to the closed-loop system for $t \in [t_k, t_{k+1})$. Eq. 3.5a defines a quadratic cost index penalizing state and manipulated input deviation from an operating steady-state which should be minimized. Eqs. 3.5b-3.5c are used to predict the future evolution of the nominal model of the system of Eq. 2.39. Eq. 3.5d represents the process constraints that must be satisfied along the prediction

horizon. Eq. 3.5e accounts for the constraints on the available control energy computed by LMPC. Eq. 3.5f-3.5g accounts for the manipulated inputs regulated by the PI controllers and the manipulated inputs that are fixed, respectively. Eq. 3.5h provides the initial state for the predicted state trajectories which is a measurement of the actual system state. The constraint of Eq. 3.5i ensures that the time derivative of the Lyapunov function at the initial sampling time (first move) of LMPC is less than or equal to the time derivative of the Lyapunov function obtained if the Lyapunov-based controller $\hat{h}(x)$ is implemented in the closed-loop system in a sample-and-hold fashion. Through this constraint, the LMPC inherits the stability and robustness properties of the Lyapunov-based controller (the reader may refer [27, 28] for more discussion and analysis on this issues). The control actions that are applied to the closed-loop system under the LMPC are defined as follows:

$$u_i(t) = u_i^*(t|t_k),\ i = 1, ..., 5,\ \forall\, t \in [t_k, t_{k+1}).$$

3.6 Lyapunov-based economic model predictive control

Optimization of a chemical process operation with respect to general economic considerations has received extensive attention. Within process control, one control scheme that addresses both dynamic economic optimization and process control is economic model predictive control. In our previous work [12], we introduced an economic model predictive control scheme designed via Lyapunov techniques for nonlinear systems. The formulation

of the LEMPC applied to the vinyl acetate process network of Eq. 2.39 is:

$$\max_{u_1,\ldots,u_5\in S(\Delta)} \int_{t_k}^{t_{k+N}} L(\tilde{x}(\tilde{\tau}), u_1(\tilde{\tau}), \ldots, u_{20}(\tilde{\tau}))d\tilde{\tau} \tag{3.6a}$$

$$\text{s.t. } \dot{\tilde{x}}(t) = f(\tilde{x}(t), u_1(t), \ldots, u_{20}(t)) \tag{3.6b}$$

$$0 = g(\tilde{x}(t), u_1(t), \ldots, u_{20}(t)),\ \forall\, t \in [t_k, t_{k+N}) \tag{3.6c}$$

$$0 \leq h(\tilde{x}(t), u_1(t), \ldots, u_{20}(t)),\ \forall\, t \in [t_k, t_{k+N}) \tag{3.6d}$$

$$u_i(t) \in U_i,\ i = 1, \ldots, 13,\ \forall\, t \in [t_k, t_{k+N}) \tag{3.6e}$$

$$u_i(t) = u_{PI,i}(t),\ i = 6, \ldots, 13,\ \forall\, t \in [t_k, t_{k+N}) \tag{3.6f}$$

$$u_i(t) = u_i^{fixed},\ i = 14, \ldots, 20,\ \forall\, t \in [t_k, t_{k+N}) \tag{3.6g}$$

$$\tilde{x}(t_k) = x(t_k) \tag{3.6h}$$

$$V(\tilde{x}(t)) \leq \tilde{\rho},\ \forall\, t \in [t_k, t_{k+N}),\ \text{if } t_k \leq t' \text{ and } V(x(t_k)) \leq \tilde{\rho} \tag{3.6i}$$

$$\begin{aligned} &\frac{\partial V(x)}{\partial x} f(x(t_k), u_1(t_k), \ldots, u_5(t_k), u_{PI,6}(t_k), \ldots, u_{PI,13}(t_k), u_{14}^{fixed}, \ldots, u_{20}^{fixed}) \\ &\quad \leq \frac{\partial V(x)}{\partial x} f(x(t_k), \hat{h}_1(x(t_k)), \ldots, \hat{h}_5(x(t_k)), u_{PI,6}(t_k), \ldots, u_{PI,13}(t_k), \\ &\qquad\qquad u_{14}^{fixed}, \ldots, u_{20}^{fixed}) \qquad \text{if } t_k > t' \text{ or } \tilde{\rho} < V(x(t_k)) \leq \rho \end{aligned} \tag{3.6j}$$

where $S(\Delta)$ is the family of piece-wise constant functions with sampling time Δ, N is the prediction horizon, $L(\tilde{x}(\tilde{\tau}), u_1(\tilde{\tau}), ..., u_m(\tilde{\tau}))$ is the economic measure which defines the objective function, $\tilde{x}$ is the predicted state trajectory of the nominal system with inputs $1, \ldots, 5$ computed by the LEMPC, $6, \ldots, 13$ computed by the PI controllers, and fixed inputs u_i^{fixed} for inputs $i = 14, \ldots, 20$, and initial state $x(t_k)$. The optimal solution to this optimization problem is denoted by $u_i^*(\tilde{\tau}|t_k)$ which is defined for $\tilde{\tau} \in [t_k, t_{k+N})$.

Eq. 3.6a defines the economic cost index which should be optimized for the process. The constraints of Eqs. 3.6b-3.6h are the same as the constraints of Eqs. 3.5b-3.5h, respectively, given in the LMPC optimization problem of Eq. 3.5. The constraints of Eq. 3.6i-3.6j are used to define the two operation modes of the LEMPC. The first operation mode is realized while the constraint of Eq. 3.6i is active. During the time period of the first operation mode (e.g., $t \leq t'$), the LEMPC operates the closed-loop system in a possible time-varying

fashion while maintaining the predicted state along the prediction horizon in a predefined set $\Omega_{\tilde{\rho}}$ to optimize the economic cost function. The second operation mode is realized while the constraint of Eq. 3.6j is active. The second operation mode corresponds to operation in which the process is driven by the LEMPC to a steady-state. We note that Ω_ρ, which is a level set of the Lyapunov function $V(x)$, is used to estimate the stability region (e.g., region of attraction) of the closed-loop system under the Lyapunov-based controller $\hat{h}(x)$, $\Omega_{\tilde{\rho}}$ is a subset of Ω_ρ that defines the safe set of operation in which the LEMPC, operating in mode 1, may optimize the economic objective freely, and t' is the switching time between mode 1 and mode 2 (e.g., t' can be an integer multiple of the sampling time of the MPC). The switching time t' may be chosen to be arbitrarily large such that the process network is always operated under the LEMPC operating in mode 1 or it may be chosen to manage the trade-off between dynamically optimal process operation and excessive wear on control actuators required to operate a process in a time-varying fashion. If the state leaves the set $\Omega_{\tilde{\rho}}$, the operation mode of the LEMPC switches to mode 2 operation.

Even though the LEMPC is formulated with an economic cost function to address both process control and dynamic economic optimization of a nonlinear system, no guarantee can be made that the closed-loop economic performance under LEMPC operating mode 1 (possibly leading to time-varying operation) will be better compared to the closed-loop economic performance under LMPC. This issue will be addressed in the subsequent section. In contrast, Heidarinejad et al. [13] recently proposed LEMPC algorithms to ensure improved economic performance under LEMPC where an auxiliary LMPC was used to formulate constraints in the LEMPC optimization problem that guarantee that the closed-loop economic performance with LEMPC be at least as good as LMPC while ensuring the LEMPC uses the same amount of control energy as the LMPC (we refer the reader to [13] for detailed results).

Remark 4 *The region $\Omega_{\tilde{\rho}}$ is chosen such that LEMPC optimization problem of Eq. 3.6 remains feasible for any $x(t) \in \Omega_\rho$, $t \geq 0$. Specifically, if $x(t) \in \Omega_\rho \setminus \Omega_{\tilde{\rho}}$, the LEMPC*

operates in mode 2 to force the process state to $\Omega_{\tilde{\rho}}$. Once the process state has converged to the set $\Omega_{\tilde{\rho}}$ and $t \leq t'$, the LEMPC operates in mode 1. The process state may come out of $\Omega_{\tilde{\rho}}$ over one sampling period while the LEMPC is operating in mode 1, but $\Omega_{\tilde{\rho}}$ is chosen to be sufficiently small such that the process state will not come out of Ω_ρ before the next sampling period. At the next sampling period, the LEMPC operates in mode 2 to force the process state back to $\Omega_{\tilde{\rho}}$. Therefore, the LEMPC optimization problem always remains feasible for any $x(t) \in \Omega_\rho$; see ref [12] for a detailed proof of this issue.

Remark 5 *If the switching time $t' = 0$, the LEMPC always operates in mode 2 and will force the process state to converge to a small neighborhood of the steady-state.*

Chapter 4

Application of MPC to the vinyl acetate process

4.1 Simulation results

In this section, we implement the two model predictive control structures: the LMPC of Eq. 3.5 and the LEMPC of Eq. 3.6 on the vinyl acetate process network. The simulations are conducted using JAVA programming environment with an Intel® Core™2 Quad Q6600 computer. Explicit Euler integration method is used to integrate the nonlinear dynamic process model of Eq. 2.39a with a fixed integration step size equal to 0.001 minutes. The integration step size is chosen to ensure stable numerical integration and sufficient accuracy of the numeric integration. The open source interior point optimizer IPOPT [33] is used to solve the optimization problems. The prediction horizon of $N = 5$ is chosen for the LMPC and the LEMPC. The first optimized control inputs computed by the optimization problems are applied to the process every sampling time (Δ) following a receding horizon scheme.

In this work, we initially demonstrate that LMPC is capable of driving the closed-loop system to the unstable steady-state that corresponds to the steady-state input listed

in Table 2.4 from an initial state. The steady-state and steady-state input denoted as x_s, u_s, respectively, have been chosen to satisfy the process (state and input) constraints. The evolution of the Lyapunov function of the closed-loop process network over a 300 min. simulation is shown in Figure 4.1. Since the magnitude of the Lyapunov function is initially large, the Lyapunov function is plotted on a semi-logarithm scale in order to observe the descending trajectory of the Lyapunov function throughout the simulation.

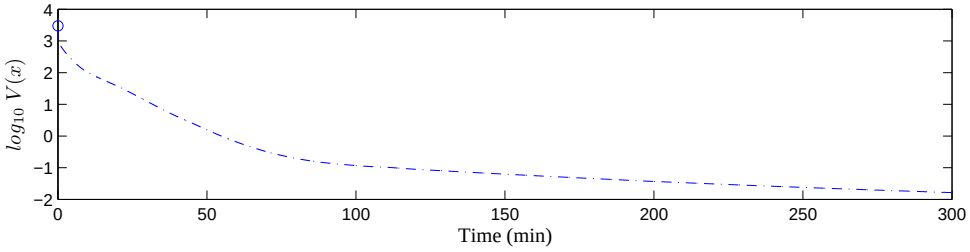

Figure 4.1: Trajectory of logarithm of the Lyapunov function $V(x)$ under LMPC.

The region Ω_ρ is approximately calculated by extensive closed-loop simulations under LMPC by initializing the process network at different initial states. From these simulations, the region Ω_ρ is defined as the level set Ω_ρ with $\rho = 5600$ which has been taken as the largest level set of the Lyapunov function where the Lyapunov function under LMPC is decreasing over each sampling period for any initial state starting inside Ω_ρ. Subsequently, we define the parameter $\tilde{\rho}$ through a series of closed-loop simulations under LEMPC operating in mode 1 only. The region $\Omega_{\tilde{\rho}}$ is the subset of the stability region Ω_ρ used in the formulation of LEMPC of Eq. 3.6 (i.e., the set where the process network is allowed to evolve when LEMPC is operating in mode 1) . The procedure for determining $\tilde{\rho}$ is as follows: starting from $\tilde{\rho} = \rho = 5600$, $\tilde{\rho}$ is decreased until the LEMPC maintains stability of the process network (i.e., boundedness of the state inside of $\Omega_{\tilde{\rho}}$). Through this procedure, the parameter $\tilde{\rho}$ used in the formulation of the LEMPC is $\tilde{\rho} = 3275$.

The LEMPC, operating in mode 1 only, is applied to operate the process network in a possible time-varying (transient) manner as to optimize the economic cost while maintaining

the process states inside $\Omega_{\tilde{\rho}}$. The Lyapunov-based constraint of the LEMPC (Eq. 3.6i) is formulated with the Lyapunov function based on the steady-state x_s and the parameter $\tilde{\rho} = 3275$. The process network under LEMPC is initialized at the same state as the closed-loop system under LMPC demonstrated in Figure 4.1. The closed-loop input and state trajectories under LEMPC over the entire 300 min. simulation are shown in Figures 4.2 and 4.3, respectively. The transient input and state profiles are shown over the first 10 min. of the simulation in Figures 4.4 and 4.5, respectively. From Figure 4.2, the LEMPC operates the process network in a time-varying manner (continuously changing control actions being computed for manipulated inputs on LEMPC). However, since the input trajectories change at a high frequency to maintain the process as close as possible to an economically optimal steady-state, the observed behavior of the closed-loop process state is similar to steady-state operation (Figure 4.3). The high frequency fluctuations (appearing as chattering in the plots) in the computed input profiles by the LEMPC occur because the LEMPC is formulated with an economic cost that does not explicitly depend on the manipulated inputs and the LEMPC (operating in mode 1) does not include a constraint that imposes convergence to a steady-state (this chattering behavior can be eliminated if LEMPC mode 2 is implemented and this has been verified in the present case via simulations).

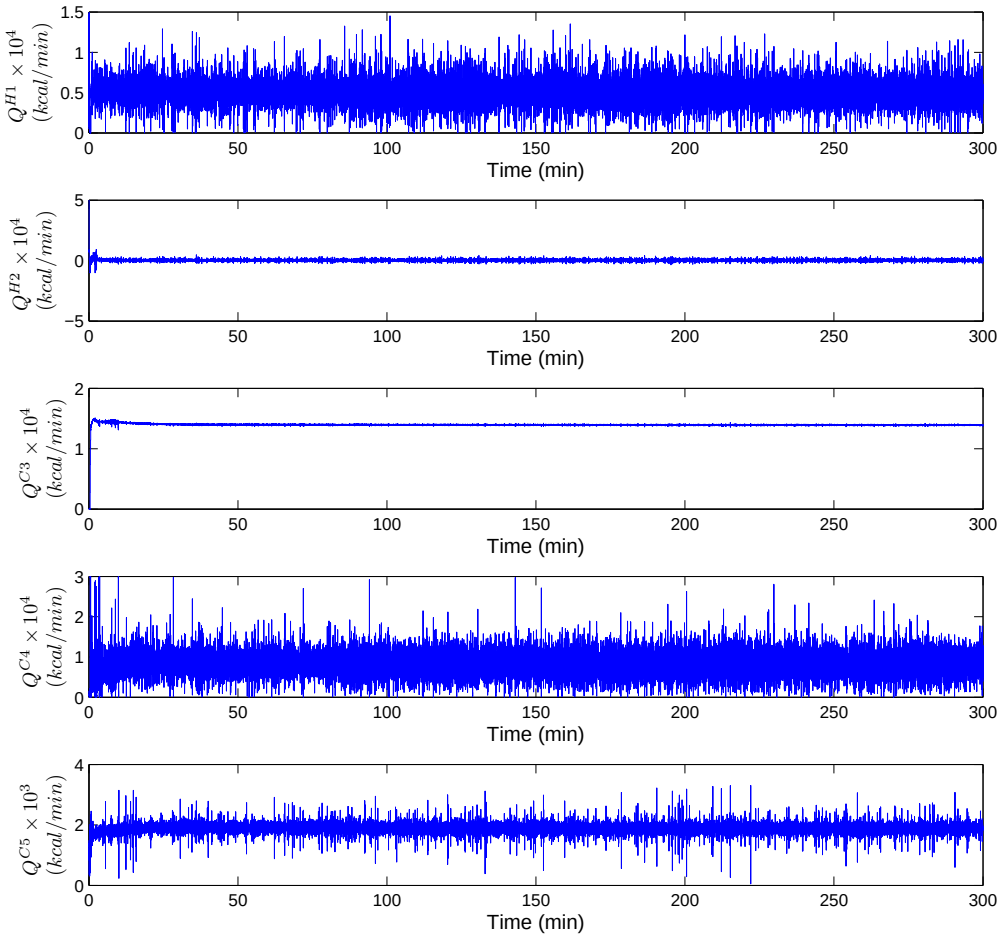

Figure 4.2: Trajectories of the manipulated inputs for heaters and coolers under LEMPC.

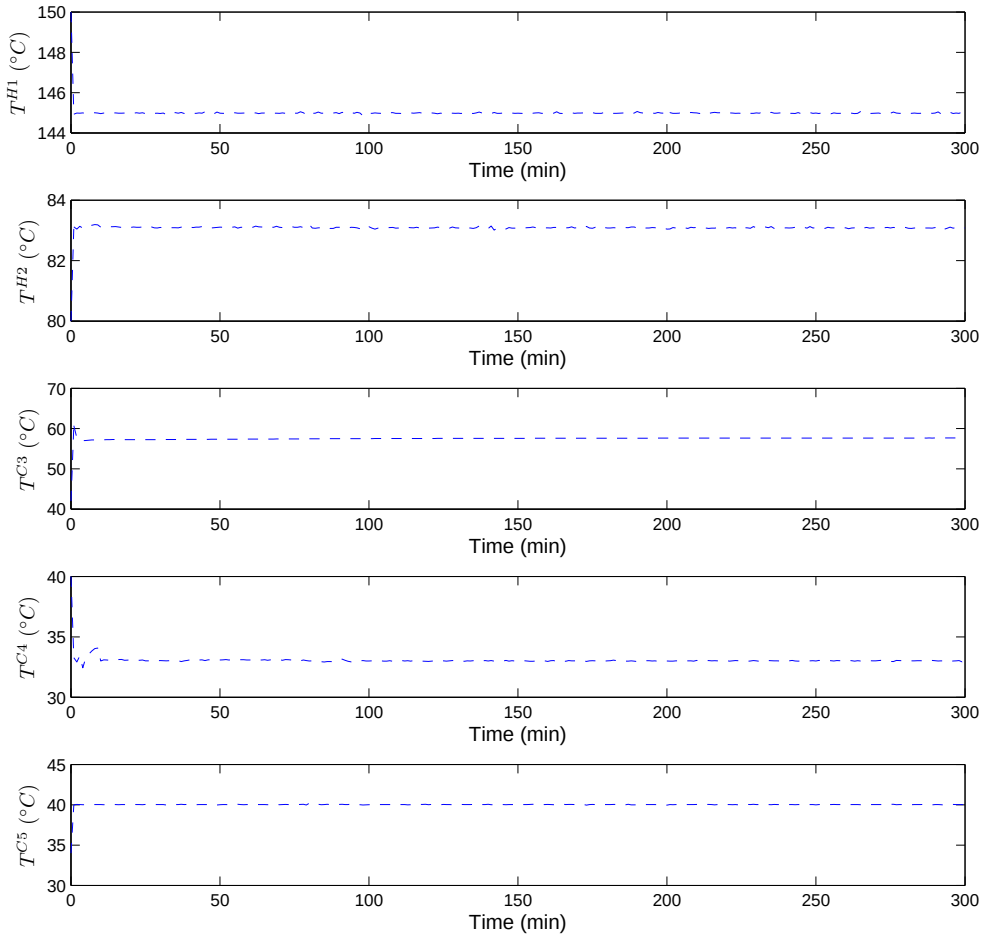

Figure 4.3: Closed-loop state trajectories under LEMPC of the heaters and coolers.

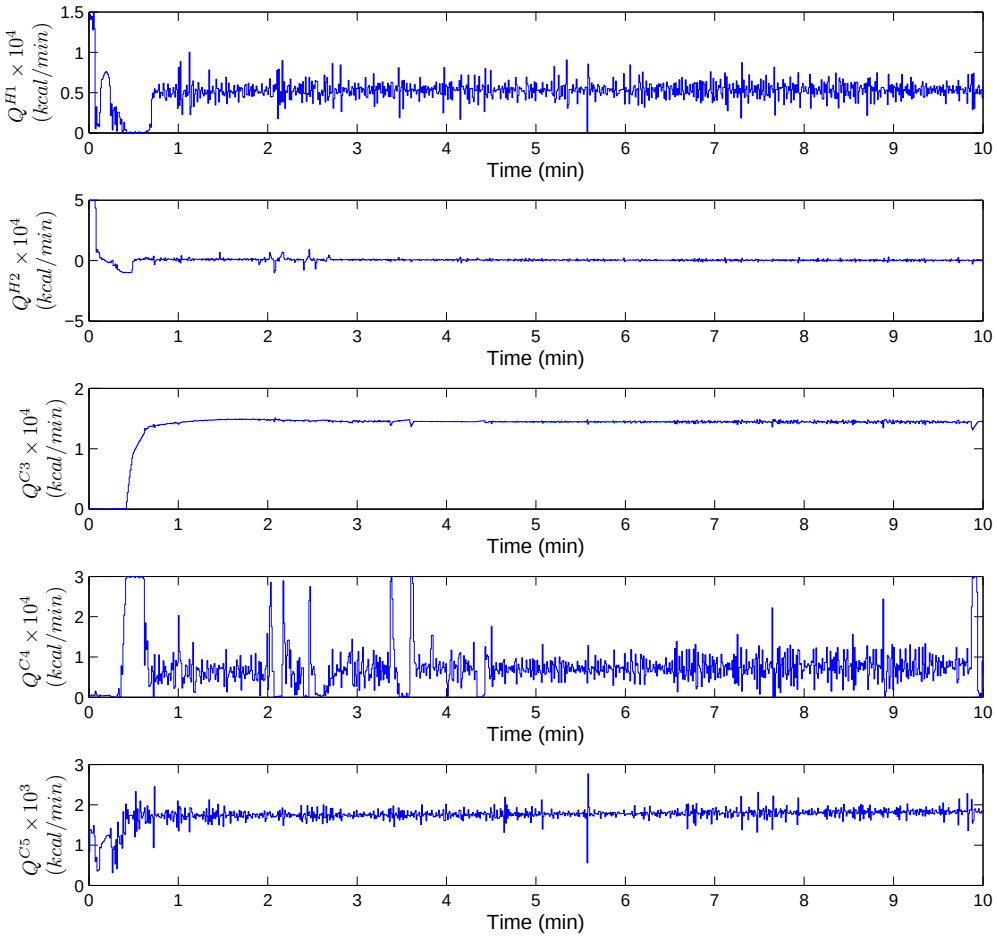

Figure 4.4: Transient trajectories of the manipulated inputs for heaters and coolers under LEMPC.

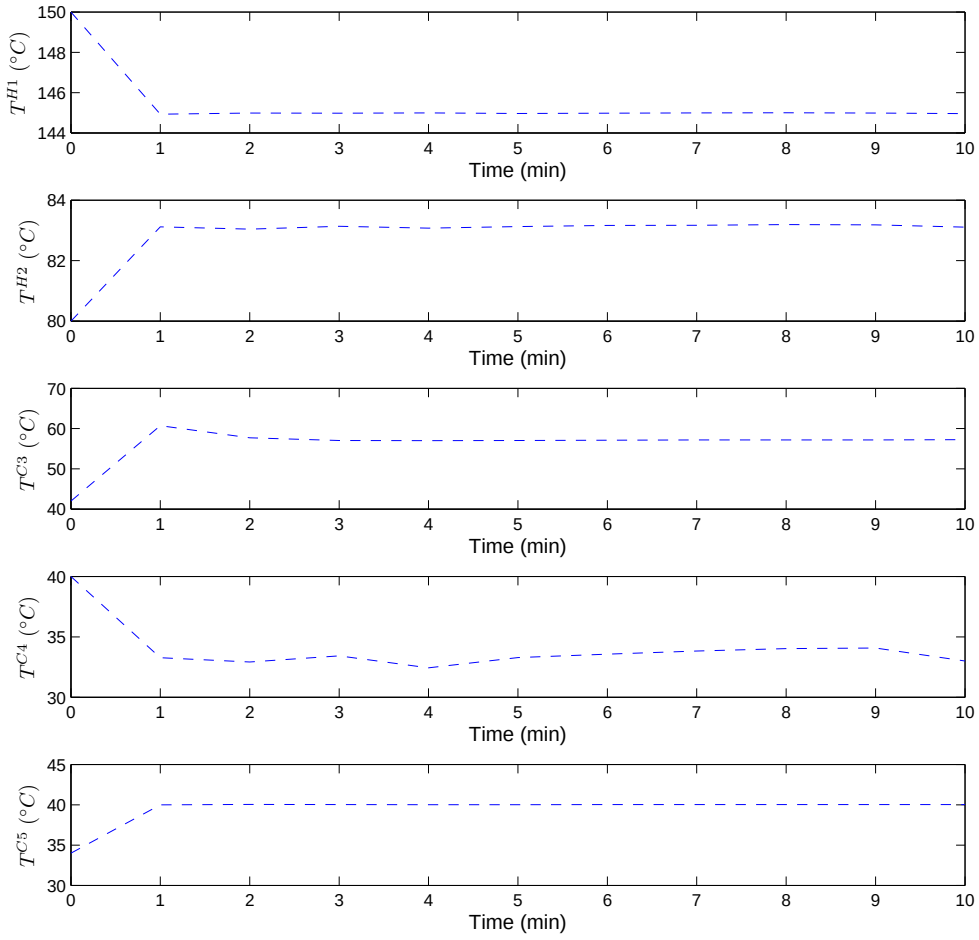

Figure 4.5: Transient closed-loop state trajectories under LEMPC of the heaters and coolers.

Compared to LMPC that forces the closed-loop process network to the steady-state x_s, LEMPC significantly decreases the duty of the cooler $C3$ which results in the low recovery of VAc in the separator as shown in Figure 4.6. Consequently, the majority of VAc from the reactor is recovered in the absorber. Figure 4.7 shows the temperature and molar fraction of VAc profiles of the absorber at each stage at the end of simulation under LMPC and LEMPC and points out that the evolution of the closed-loop system under LMPC is different from the evolution of the closed-loop system under LEMPC.

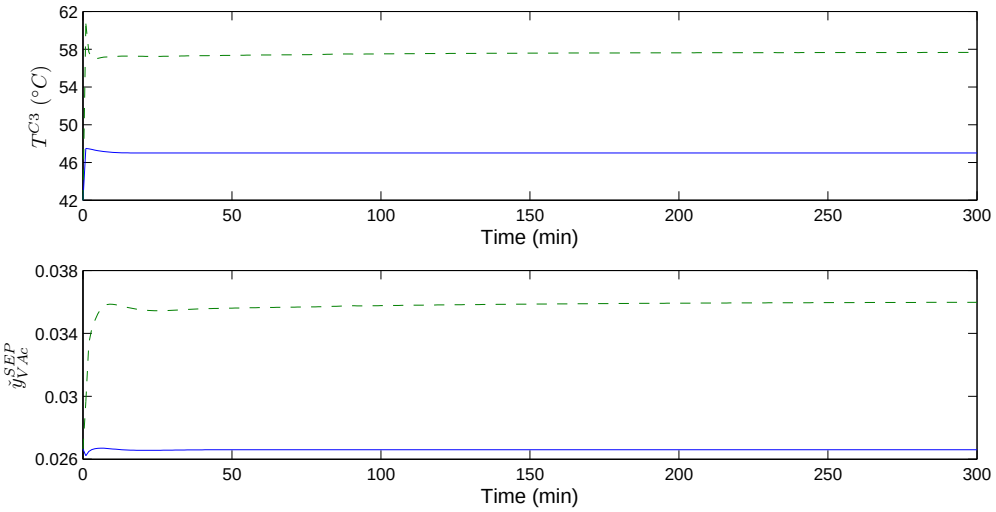

Figure 4.6: State trajectories of the temperature of the cooler prior to the separator (top plot) and state trajectories of the vapor phase vinyl acetate composition in the separator (bottom plot) with LMPC (solid line) and with LEMPC (dashed line).

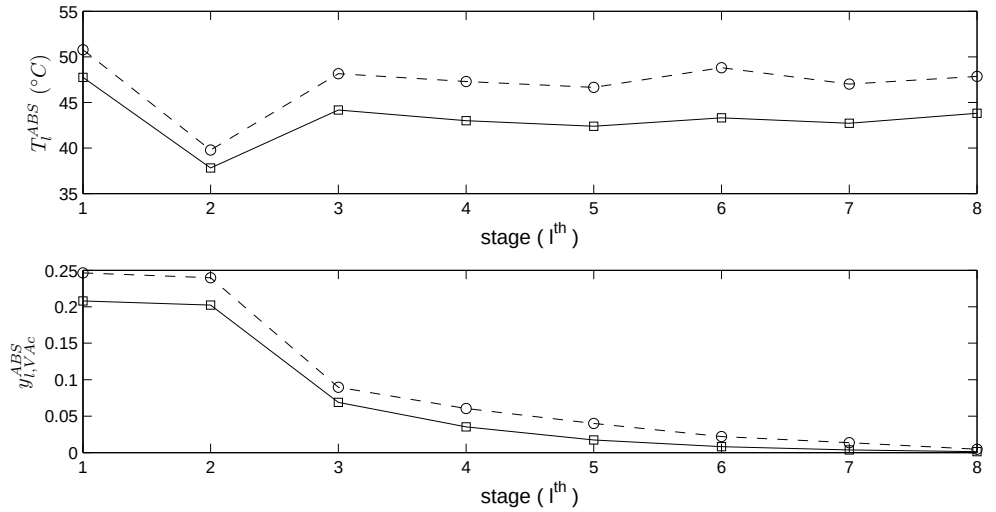

Figure 4.7: The temperature (top plot) and VAc concentration (bottom plot) profiles of the absorber at each stage under LMPC (square) and under LEMPC (circle) at the end of simulation.

Since the closed-loop process network under LEMPC evolves like steady-state operation, we compare the closed-loop economic performance of the process network under LEMPC

with the closed-loop economic performance of the process network under LMPC formulated with the operating steady-state of the LEMPC denoted as x_s^* with corresponding steady-state input u_s^*. The steady-state x_s^* is defined from the closed-loop simulation of the process network under LEMPC. Since the control actions computed by the LEMPC and the corresponding state profiles have significant fluctuations as displayed in Figures 4.2-4.3, x_s^* and u_s^* are computed by averaging out the profiles of the state and inputs over the last 10 minutes of the simulation to determine the operating steady-state under LMPC. In this manner, the RTO layer (upper-layer economic steady-state optimization) for the closed-loop process network under LMPC is the LEMPC that provides the optimal steady-state by averaging the state profiles. To compare the closed-loop economic performance of the process network under LMPC and LEMPC, we initialize the process network at the same initial state and define the average total economic measure (J_e) over two 300 min. closed-loop simulations as

$$J_e = \frac{1}{t_f} \sum_{k=0}^{f} L(t_k) \tag{4.1}$$

where $t_k = k\Delta$, $k = 0, 1, ..., f$.

Figures 4.8 and 4.9 show the closed-loop input and state trajectories of the process network under LMPC over the entire 300 min. simulation; while, Figures 4.10 and 4.11 show the closed-loop input and state trajectories over the first 10 min. Figure 4.12 shows the trajectories of the economic measure under LEMPC and LMPC, in which the average economic performance of the closed-loop system under LEMPC (576.6) is not better than the average economic performance of the closed-loop system under LMPC (576.8). Indeed, the formulation of LEMPC (operating in mode 1 only) utilized in this work does not ensure improved economic performance of LEMPC over LMPC. As observed in Figure 4.2 and Figure 4.8, LEMPC, operating in mode 1, allows for unfavorable and impractical trajectories of control inputs compared to the trajectories of control inputs computed by LMPC. In addition, LEMPC requires significantly larger evaluation time than LMPC (on the order of days).

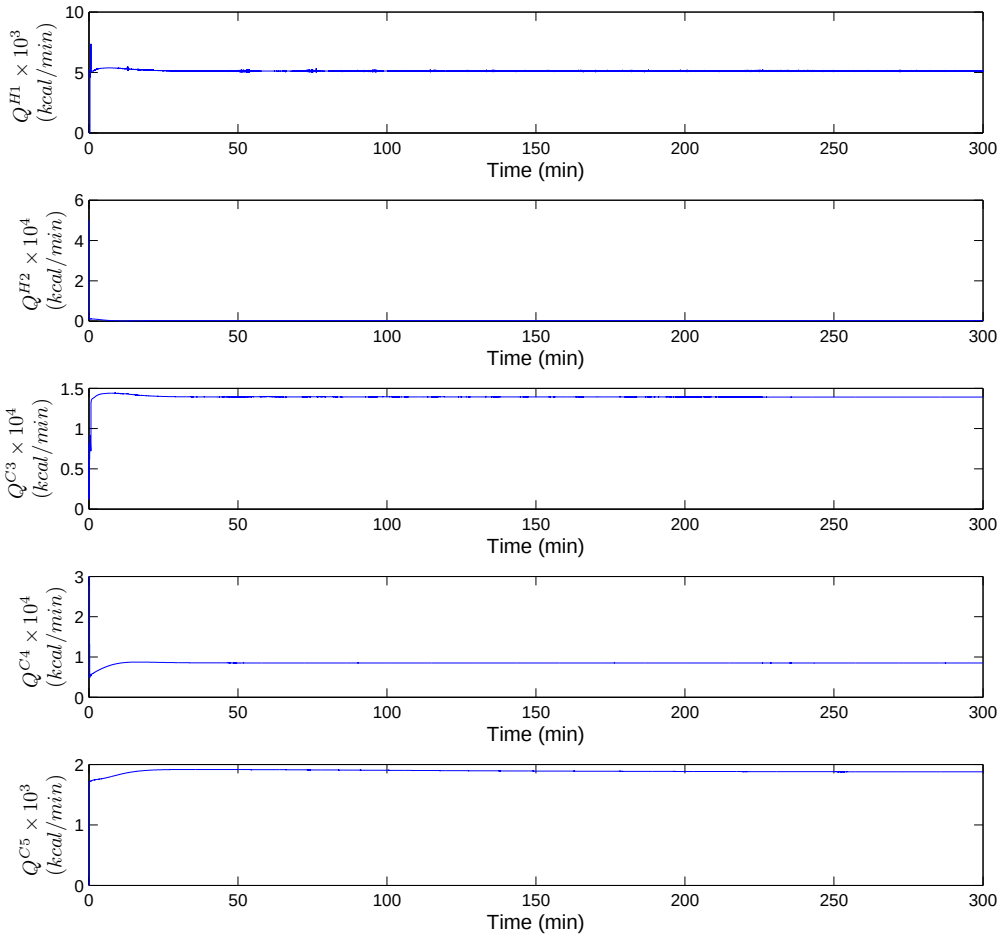

Figure 4.8: Trajectories of the manipulated inputs for heaters and coolers under LMPC.

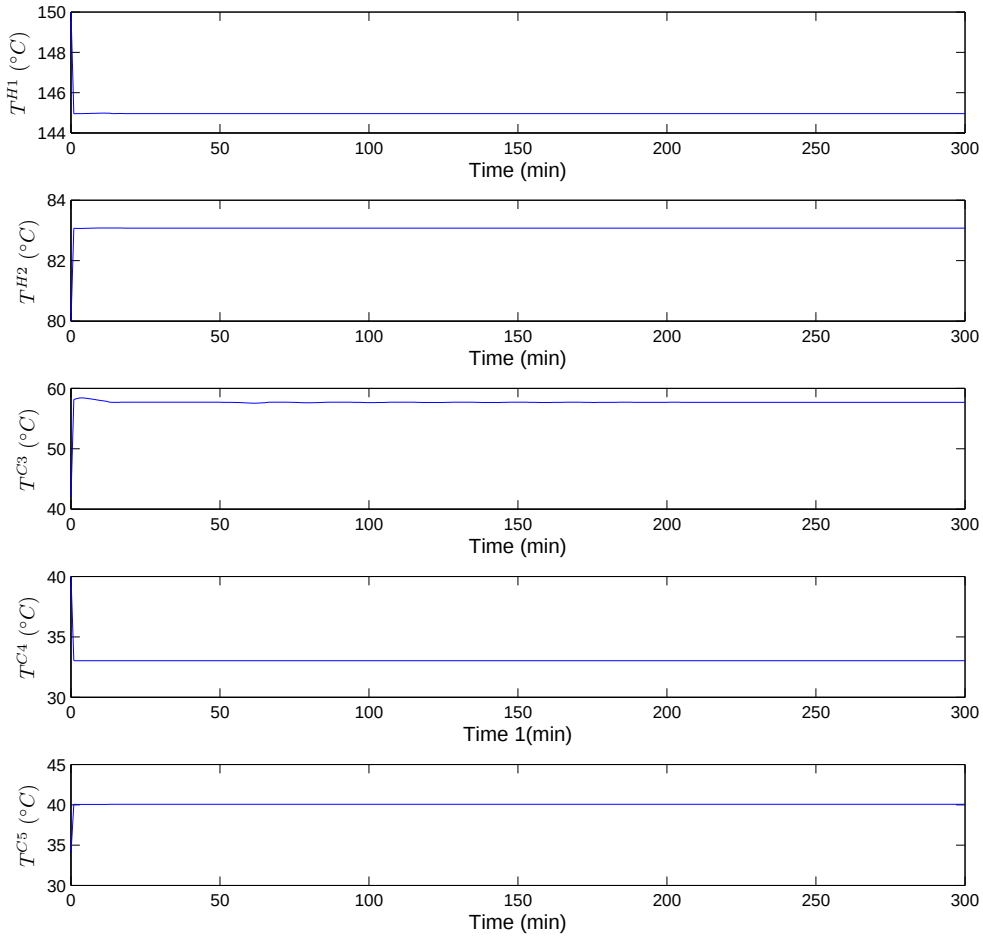

Figure 4.9: Closed-loop state trajectories under LMPC of the heaters and coolers.

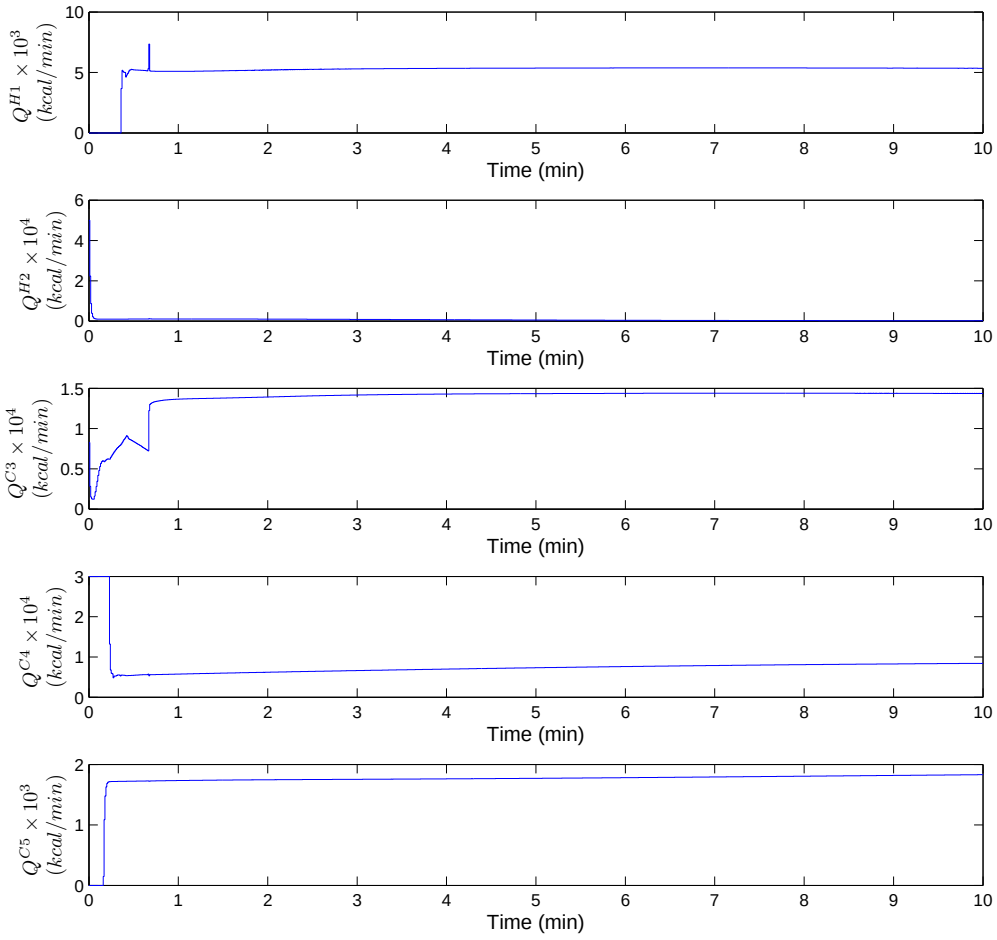

Figure 4.10: Transient trajectories of the manipulated inputs for heaters and coolers under LMPC.

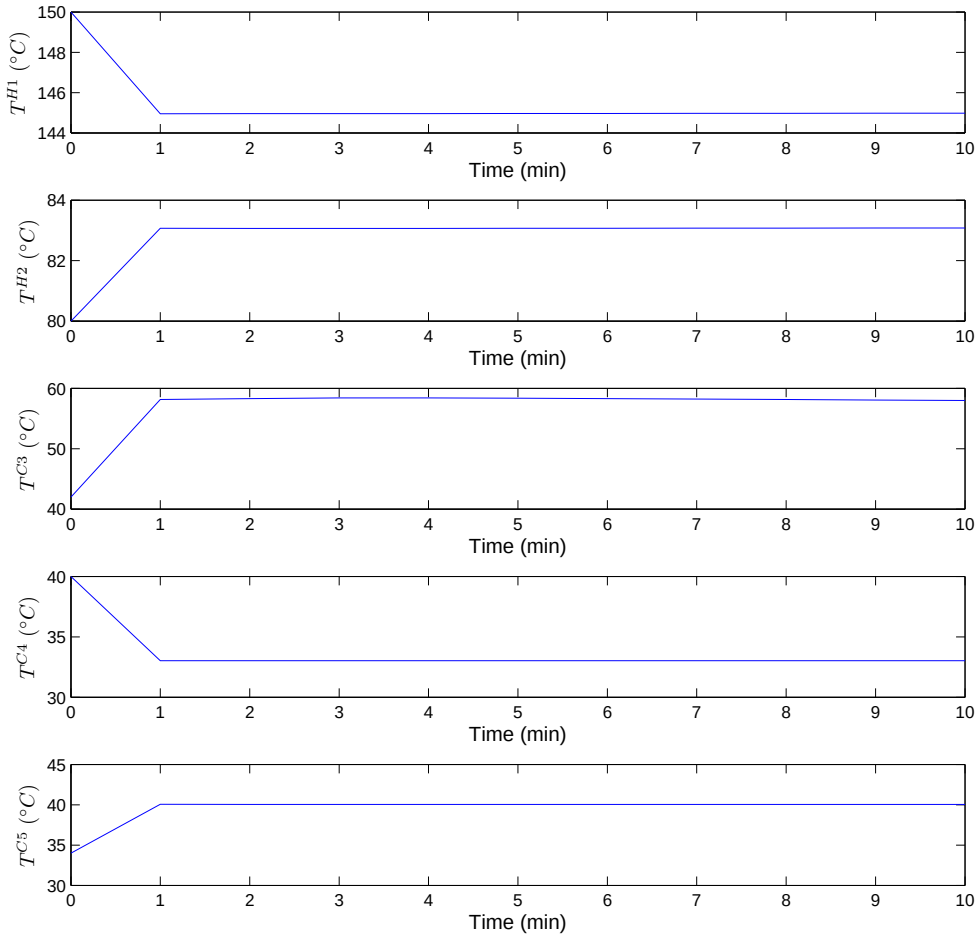

Figure 4.11: Transient closed-loop state trajectories under LMPC of the heaters and coolers.

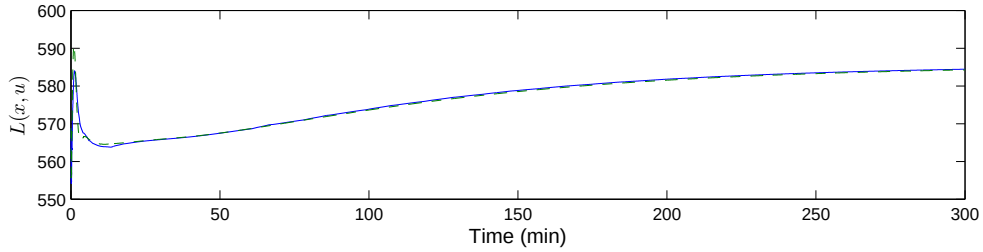

Figure 4.12: Trajectories of the economic measure under LMPC (solid line) and under LEMPC (dashed line).

4.2 When is EMPC needed?

In this work, we applied LMPC and LEMPC to a vinyl acetate process network. The closed-loop economic performance of two simulations under LMPC and LEMPC were similar. This raises an important question when considering the application of EMPC to a chemical process network: When is EMPC needed? With large-scale process networks such as the vinyl acetate process network, operating process networks in a time-varying fashion as to optimize economic measures while meeting process constraints is difficult because the dynamics of each unit are coupled to the dynamics of the other units through the recycle streams. While the topic of guaranteed closed-loop economic performance has been addressed in ref [13], if we apply the LEMPC introduced in ref [13] to this particular large-scale chemical process network, the LEMPC would compute control actions that would approach the auxiliary LMPC. The computational requirement for solving the LEMPC and LMPC problems in such control framework would not likely be offset by the little improvement in closed-loop economic performance. Therefore, the best operating strategy for large-scale chemical process networks with coupling of process dynamics would likely be operating at the economically optimal steady-state. Since process networks are typically operated continuously for long periods of time, the objective of the controller formulated for steady-state operation is to drive and regulate the process network to a steady-state and the effect of the transient state becomes insignificant on closed-loop economic performance. Hence, the difference in economic closed-loop performance of the process network under LMPC formulated with a conventional quadratic cost and under LEMPC formulated with the economic cost function, but operating in mode 2, will also be insignificant if operation can be maintained at the steady-state (bound on the disturbances is small).

If there exists any time-varying operating strategy that is better than operating at the economically optimal steady-state, then one would have to increase the prediction horizon of the LEMPC in an attempt to improve closed-loop economic performance. The computa-

tional cost of increasing the horizon may make, however, EMPC impractical to implement. One may consider the closed-loop economic performance of the process network under the other formulations of EMPC in the literature like, for instance, the EMPC studied in refs [1, 7] where a terminal constraint is used in the formulation instead of the Lyapunov-based constraint of Eq. 3.6i in LEMPC. However, the Lyapunov-based constraint allows the LEMPC to operate the system in a time-varying fashion while maintaining the state inside a subset of the estimated closed-loop stability region as opposed to the EMPC with terminal constraint which allows the EMPC to operate the system in a time-varying fashion as long as the system is forced to the operating steady-state at the end of the prediction horizon. Therefore, the terminal constraint is, in some sense, more restrictive in terms of the available time-varying operating trajectories. For this reason, it is also unlikely that using EMPC with a terminal constraint will provide significant economic closed-loop performance improvement in this example compared to MPC formulated with a conventional quadratic cost.

The main advantage of EMPC is when it operates a process in a time-varying (transient) fashion to yield better closed-loop economic performance. Clearly, some processes do not benefit from time-varying operation based on the intrinsic properties of the dynamics. However, these systems may still benefit from application of EMPC if the economic cost function and constraints become time-varying (e.g., the weights A_1, A_2, and A_3 of the economic cost become time-varying). Time-varying economic cost and constraints allows LEMPC to fully manipulate process capacities to meet the continuously changing market demand, feedstock variability and energy cost.

Chapter 5

Conclusions

In this work, two Lyapunov-based MPC schemes are developed and applied to a large-scale chemical process network used in the production of vinyl acetate. The nonlinear dynamic process network consists of 179 nonlinear differential equations and 13 manipulated inputs and is composed of process units such as a vaporizer, a separator, a plug-flow reactor, a gas-liquid absorber, a process-to-process heat exchanger, and heaters/coolers. Specifically, we propose an economic measure accounting for the reaction selectivity in the reactor and the separation quality of vinyl acetate in the separator and the absorber. Subsequently, a novel control architecture which comprises of a LMPC/LEMPC acting to regulate 5 manipulated inputs which directly influence in the economic measure and a set of PI controllers acting to regulate the other manipulated inputs to maintain closed-loop stability is applied to the process network. The economic performance of the closed-loop system under LMPC formulated with a conventional quadratic cost function associated with the system steady-state is compared with the economic performance of the closed-loop system under LEMPC which explicitly considers an economic measure as its objective function through extensive simulations. After a thorough comparison and analysis, we found that operating the process network under LMPC leads to similar closed-loop economic performance as operating the process network under LEMPC (operating in mode 1 only). Furthermore, operating the

process network in a time-varying fashion under LEMPC (mode 1) leads to operation at an economically optimal steady-state. In a future work, we can adopt time-varying economic cost and constraints in LEMPC design to address the continuously changing economic objectives and constraints such as the changing market demand on vinyl acetate.

Bibliography

[1] D. Angeli, R. Amrit, and J. B. Rawlings. On average performance and stability of economic model predictive control. *IEEE Transactions on Automatic Control*, 57:1615–1626, 2012.

[2] T. Backx, O. Bosgra, and W. Marquardt. Integration of model predictive control and optimization of processes: enabling technology for market driven process operation. In *Proceedings of the IFAC Symposium on Advanced Control of Chemical Processes*, pages 249–260, Pisa, Italy, 2000.

[3] R. B. Bird, W. E. Stewart, and E. N. Lightfoot. *Transport Phenomena*. John Wiley & Sons, 1960.

[4] S. P. Burke and W. B. Plummer. Gas flow through packed columns. *Industrial & Engineering Chemistry*, 20:1196–1200, 1928.

[5] R. Chen, K. Dave, T. J. McAvoy, and M. Luyben. A nonlinear dynamic model of a vinyl acetate process. *Industrial & Engineering Chemistry Research*, 42:4478–4487, 2003.

[6] P. D. Christofides and N. H. El-Farra. *Control of Nonlinear and Hybrid Process Systems: Designs for Uncertainty, Constraints and Time-Delays*. Springer-Verlag, Berlin, Germany, 2005.

[7] M. Diehl, R. Amrit, and J. B. Rawlings. A Lyapunov function for economic optimizing model predictive control. *IEEE Transactions on Automatica Control*, 56:703–707, 2011.

[8] N. H. El-Farra and P. D. Christofides. Bounded robust control of constrained multivariable nonlinear processes. *Chemical Engineering Science*, 58:3025–3047, 2003.

[9] S. Engell. Feedback control for optimal process operation. *Journal of Process Control*, 17:203–219, 2007.

[10] C. E. Garcia, D. M. Prett, and M. Morari. Model predictive control: Theory and practice-a survey. *Automatica*, 25:335–348, 1989.

[11] B. Gebhart. *Heat Transfer*. McGraw-Hill, second edition, 1971.

[12] M. Heidarinejad, J. Liu, and P. D. Christofides. Economic model predictive control of nonlinear process systems using Lyapunov techniques. *AIChE Journal*, 58:855–870, 2012.

[13] M. Heidarinejad, J. Liu, and P. D. Christofides. Algorithms for improved fixed-time performance of Lyapunov-based economic model predictive control of nonlinear systems. *Journal of Process Control*, 23:404–414, 2013.

[14] R. Huang, E. Harinath, and L. T. Biegler. Lyapunov stability of economically-oriented NMPC for cyclic processes. *Journal of Process Control*, 21:501–509, 2011.

[15] A. N. E. Idris and S. Engell. Economics-based NMPC strategies for the operation and control of a continuous catalytic distillation process. *Journal of Process Control*, 22:1832–1843, 2012.

[16] J. V. Kadam and W. Marquardt. Integration of economical optimization and control for intentionally transient process operation. In R. Findeisen, F. Allgöwer, and L. T. Biegler, editors, *Assessment and Future Directions of Nonlinear Model Predictive Con-*

trol, volume 358 of *Lecture Notes in Control and Information Sciences*, pages 419–434. Springer Berlin / Heidelberg, 2007.

[17] P. Kokotovic and M. Arcak. Constructive nonlinear control: a historical perspective. *Automatica*, 37:637–662, 2001.

[18] Y. Lin and E. D. Sontag. A universal formula for stabilization with bounded controls. *Systems & Control Letters*, 16:393–397, 1911.

[19] Y. Lin, E. D. Sontag, and Y. Wang. A smooth converse Lyapunov theorem for robust stability. *SIAM Journal on Control and Optimization*, 34:124–160, 1996.

[20] M. Luyben and B. Tyres. An industrial design/control study for the vinyl acetate monomer process. *Computers & Chemical Engineering*, 22:867, 1998.

[21] W. Luyben. Design and control of a modified vinyl acetate monomer process. *Industrial & Engineering Chemistry Research*, 50:10136–10147, 2011.

[22] W. Luyben, B. Tyres, and M. Luyben. *Plantwide Process Control*. McGraw Hill, 1999.

[23] J. Ma, J. Qin, T. Salsbury, and P. Xu. Demand reduction in building energy systems based on economic model predictive control. *Chemcal Engineering Science*, 67:92–100, 2011.

[24] T. E. Marlin and A. N. Hrymak. Real-time operations optimization of continuous processes. *AIChE Symposium Series on CPC V*, 93:156–164, 1997.

[25] D. Q. Mayne, J. B. Rawlings, C. V. Rao, and P. O. M. Scokaert. Constrained model predictive control: Stability and optimality. *Automatica*, 36:789–814, 2000.

[26] P. Mhaskar, N. H. El-Farra, and P. D. Christofides. Predictive control of switched nonlinear systems with scheduled mode transition. *IEEE Transactions on Automatic Control*, 50:1670–1680, 2005.

[27] P. Mhaskar, N. H. El-Farra, and P. D. Christofides. Stabilization of nonlinear systems with state and control constraints using Lyapunov-based predictive control. *Systems & Control Letters*, 55:650–659, 2006.

[28] D. Muñoz de la Peña and P. D. Christofides. Lyapunov-based model predictive control of nonlinear systems subject to data losses. *IEEE Transactions on Automatic Control*, 53:2076–2089, 2008.

[29] P. B. Omell and J. D. Chmielewski. IGCC power plant dispatch using infinite-horizon economic model predictive control. *Industrial & Engineering Chemistry Research*, (in press), 2013.

[30] D. G. Oslen, W. Y. Svrcek, and B. R. Young. Plantwide control study of a vinyl acetate monomer process design. *Chemical Engineering Communications*, 192:1243–1257, 2005.

[31] J. B. Rawlings and R. Amrit. Optimizing process economic performance using model predictive control. In L. Magni, D. M. Raimondo, and F. Allgöwer, editors, *Nonlinear Model Predictive Control*, volume 384 of *Lecture Notes in Control and Information Sciences*, pages 119–138. Springer Berlin / Heidelberg, 2009.

[32] J. M. Smith and H. C. Van Ness. *Introduction To Chemical Engineering Thermodynamics*. McGraw Hill, 1987.

[33] A. Wächter and L. T. Biegler. On the implementation of an interior point filter line-search algorithm for large-scale nonlinear programming. *Mathematical Programming*, 106:25–57, 2009.